STRUCTURE AND STABILITY OF CARBON MOLECULAR SIEVE MEMBRANES DERIVED FROM 6FDA:BPDA-DAM PRECURSORS

A Thesis
Presented to
The Academic Faculty

By

Samuel S. Hays

In Partial Fulfillment
Of the Requirements for the Degree
Master of Science in Chemical Engineering

Georgia Institute of Technology
August 2020

STRUCTURE AND STABILITY OF CARBON MOLECULAR SIEVE MEMBRANES DERIVED FROM 6FDA:BPDA-DAM PRECURSORS

Approved by:

Dr. William J. Koros, Advisor
School of Chemical & Biomolecular Engineering
Georgia Institute of Technology

Dr. J. Carson Meredith
School of Chemical & Biomolecular Engineering
Georgia Institute of Technology

Dr. Ryan P. Lively
School of Chemical & Biomolecular Engineering
Georgia Institute of Technology

Date Approved: June 19th, 2020

ACKNOWLEDGEMENTS

I am incredibly grateful to have had this opportunity to work with so many intelligent and kind people who have helped me get to where I am today. Georgia Tech is home to so many amazing people, and I feel very honored to have spent my B.S. and M.S. working with and learning from them.

I would first like to thank my thesis committee members: Dr. J. Carson Meredith and Dr. Ryan P. Lively. Besides serving on my thesis committee, both of these professors were incredibly important in helping me pursue further goals. They both agreed to write many, (perhaps too many), recommendation letters for Ph.D. applications, and for this I owe them a lot. Additionally, I had the privilege of taking Dr. Meredith's thermodynamics class and Dr. Lively's mass transfer class. These two classes in particular really opened my eyes to not only the challenges, but also the fun in each respective subject, and this is undoubtedly due to the way the classes were instructed.

I also would like to thank all members of the Koros group, past and present, for creating an incredible work environment. I feel very lucky to have begun my research journey here. In particular, I would like to thank Manjeshwar Kamath. Besides being a great friend to everyone and occasionally bringing in delicious food, he also was the first person to introduce me to the Koros group while I was an undergraduate student. Without him, I never would have had this amazing opportunity.

Nicholas León is another group member that I would like to thank. He was the best undergraduate student turned fellow graduate student I could have asked for. From alternating 12-hour shifts with me 24 hours a day for a few weeks to ensure timely

completion of sorption isotherms, to long conversations about Super Smash Brothers, to trying to make sense of Paul Flory's writing with me, I truly appreciate his contributions and friendship and wish him the best of luck.

I also need to thank Oishi Sanyal, (or Professor Sanyal now). I cannot thank her enough for our long, in-depth conversations of the fine details of mass transfer, her friendship, and her constant willingness to mentor. I have the utmost confidence that she will go on to become an extremely successful professor. I feel very honored to have the bragging rights of being her first, (although unofficial), graduate student.

There would be no Koros group without Dr. Koros. He has been the best advisor anyone could hope for, and I have learned so much from him. He was one of the few people that saw potential in me and helped me continue my education after my undergraduate degree, and for this I will always be thankful. Dr. Koros is one of the kindest, smartest, most hard-working people I have ever met, and I only hope that I can manage to take a fraction of those traits with me as I move to a new program.

I would also like to thank my friends outside of the lab for keeping me sane. Tom Boyle, Antonio Lee, Alex Moore, Michael Muller, Aaron Ranallo, Tommy Ristau, Raynal Singh, and Jordan Trout never failed to make me laugh and were always down for a hang.

Lastly, I would like to thank my family for their continuous support. I know I could not have done it without them. My parents, David and Jennifer Hays, have always been there for me, in good times and bad, to celebrate, mentor, and motivate. My siblings, Brooke, Jack, Gwen, and Mark are always a source of fun and long board game nights. My fiancée, Courtney Branson, has been my best friend through this entire experience, and I am tremendously excited to continue on this journey with her by my side.

TABLE OF CONTENTS

LIST OF TABLES

LIST OF FIGURES

SUMMARY

With an ever-growing demand for energy, the need for energy-efficient separation of fuel-sources becomes more apparent. Membrane implementation has been identified as a feasible technique to make existing gas separation processes more efficient. Carbon molecular sieve, (CMS), membranes have emerged over the last several years as a front-runner for industrial applications due to their high processability, high tunability, and robust performance. With that in mind, there are still obstacles facing CMS membrane implementation.

This thesis attempts to shed light on one of these key obstacles. Specifically, this work attempts to fundamentally understand the physical aging phenomenon in CMS membranes derived from 6FDA:BPDA-DAM polymer precursors. Over time, CMS permeability has been shown to decrease with a corresponding increase in permselectivity, collectively termed physical aging. In the chapters below, it is shown that this phenomenon primarily affects diffusion through the membrane, leading to the conclusion that aromatic strands comprising the membrane experience a tightening effect driven by energetic interactions.

Additionally, it is demonstrated that physical aging effects can be minimized and even reversed by increasing the concentration of sorbed constituents. It is believed that the higher concentration leads to more diffusive jumps through the aromatic strands, perturbing the energetic interactions driving them to tighten. Such aging minimization techniques are relatively simple to implement, providing a realistic way to improve the longevity of the CMS membranes.

Evidence is also presented arguing for the existence of dual-mode transport in CMS membranes. Such a model has become a common way to describe gas transport in glassy polymers. The model presented in this work, although mathematically resembling the glassy polymer model, is fundamentally different. The corresponding chapter describes a majority Langmuir environment surrounded by a minority, unorganized, continuous environment well approximated by Henry's Law sorption. This model begins to explain the lack of permeability drop observed at high membrane saturation, but still allows for sorbate competition effects. Although early, this work has the potential to allow for even further control over transport through CMS membranes, further demonstrating its immense tunability.

CHAPTER 1

INTRODUCTION

1.1 Demand for Energy-Efficient Gas Separations

It is no secret that energy demand will continue to rise as countries grow in population and further develop. It is predicted that total energy demand will grow roughly 20% between now and 2040, with demand for natural gas expected to increase the most out of available energy sources[1, 2]. This is illustrated in Figure 1.1. Natural gas and other fuel sources such as crude oil must be processed before they can be used for energy production, as these sources essentially always have some sort of contaminant present. For example, raw natural gas can have possibly 25% of its contents made up of contaminants such as CO_2, H_2O, and large organics that must be removed before combustion[3]. The rise in demand of energy will therefore coincide with a rise in demand for separations.

It has been estimated that separations account for possibly 50% of the energy consumed by industries in the U.S, leading to between 10-15% of total U.S. energy usage [2, 4]. Of this energy, roughly 80% is spent on separations involving thermal processes, such as distillation and evaporation, meaning 8-12% of total U.S. energy consumption is spent on thermal separations[5]. There is great opportunity here for more energy efficient separations, such as membranes, to significantly reduce this energy consumption. Estimates show that incorporating membranes into processes formerly requiring distillation can significantly reduce energy consumption, potentially saving roughly 1-2 quads a year, or 1-2 x 10^{15} BTU, in a best-case scenario[2, 5]. Put in perspective, the U.S.

consumed roughly 100 quads in 2019 [6]. Incorporating membranes into separation processes translates to significant energy savings.

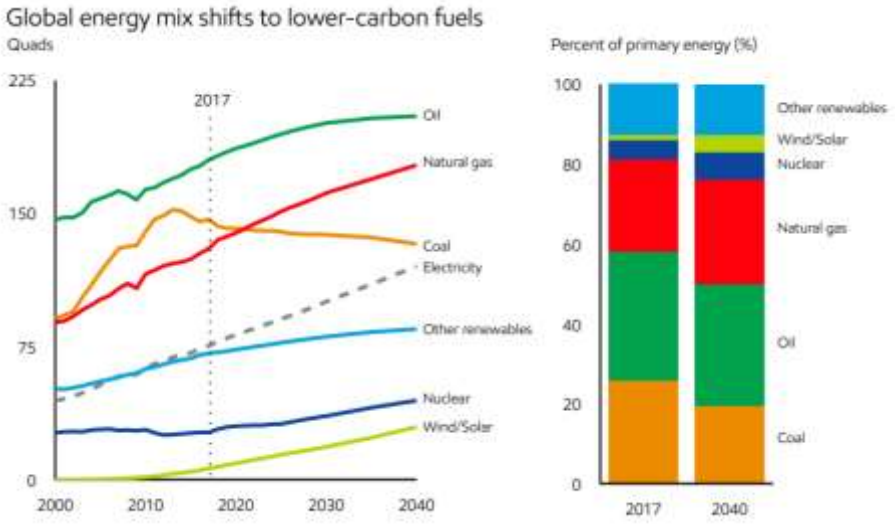

Figure 1.1. Distribution of energy demands projected to 2040 [1].

1.2 Membranes for Gas Separations

Membrane-based gas separations involve pressurizing the upstream of the membrane with the gas mixture intended on being separated, summarized in Figure 1.2. Depending on the membrane being used, different properties of the penetrants, such as size and affinity for the membrane, will determine the composition of the downstream.

Membrane research over the last several decades has demonstrated the feasibility of membrane incorporation into gas separations relying on thermal techniques[7, 8, 9, 10]. Besides being more energy efficient as discussed above, membranes also can reduce greenhouse gas emissions and reduce complexity of operating procedures[10].

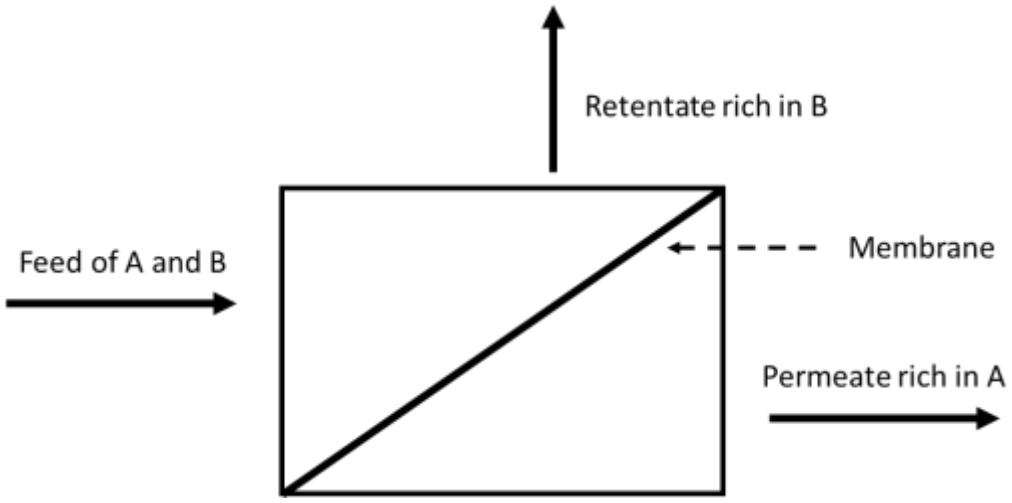

Figure 1.2. Schematic of a typical membrane gas separation.

Even with the many advantages of incorporating membranes into separation processes, membranes still comprise a small percentage of equipment used for separations. In natural gas purification, an application poised for membrane application, membranes comprise roughly 10% of the market[10]. Updating existing separation processes obviously

requires overcoming capital investment inertia, but this is a symptom of additional obstacles.

A very well-documented obstacle is the permeability-selectivity upper bound. In glassy polymer membranes, limits on the dissolution of polymers in solvents put a physical cap on achievable membrane separation properties[11, 12]. This upper bound is, in a certain way, the *ideal* limit, often based off permeabilities and selectivities of pure components on a laboratory scale. Membranes operating under industrial conditions often perform far below this upper bound with the presence of sorption competition as well as feed contaminants lowering the measured permeabilities and selectivities[9].

Additionally, plasticization of polymer membranes has also raised concerns[13, 14]. If concentrations of sorbates that have strong interactions with the particular polymer membrane are too high, the sorbates can dissolve into the polymer matrix and dilate the spaces between individual polymer chains. Such an occurrence causes significant increases in diffusion coefficients of all penetrants in the feed, increasing permeabilities but significantly lowering the selectivity of the membrane. Many steps have been taken to try and minimize this effect, such as cross-linking polymer chains to give them more rigidity, however plasticization still raises concerns.

Membrane stability is another key obstacle, and much work is being done to improve this. Over time, membrane performance can change due to various reasons, both chemical and physical. As one can imagine, performance changes, both in permeability and selectivity, may alter operation conditions of industrial processes. Ideally, the membrane, once placed into the separation process, has already been stabilized and therefore provides uniform performance over the lifetime of its usage.

Carbon molecular sieve (CMS) membranes have demonstrated they can solve some of these key problems. Because they are derived from polymer membranes, however distinctly different from them, CMS membranes can surpass the performance limitations placed on traditional glassy polymers[15, 16, 17]. Additionally, CMS membranes have demonstrated plasticization resistance, maintaining strong separation performance even under supercritical feed conditions[18]. Stability of CMS membranes has been addressed before, however not much is known about the mechanics of how the CMS changes with time. This thesis attempts to shed light on this process.

1.3 Research Objectives

Membrane stability is an important characteristic of membranes intended for industrial-level separations[9, 13]. Physical aging, or the decrease in permeability over time due to natural changes in the membrane structure, specifically has been highlighted as a key challenge facing membranes[13, 19]. As mentioned, a goal of this thesis is to outline a mechanism describing the physical aging phenomenon in CMS membranes, with the intent of allowing for design of CMS membranes to minimize physical aging effects in the future.

Additionally, this thesis aims to provide reasonable techniques capable of minimizing aging effects to current generation CMS membranes. Much is still being learned about the exciting class of CMS materials, so having techniques now that are effective at suppressing physical aging for such applications as transportation of industrial CMS modules can significantly improve the longevity of the membrane. This thesis also attempts to mechanistically explain the effectiveness of such techniques that are already in use on a laboratory scale. Specifically, storage of 6F-derived CMS membranes under 115 psia CO_2 at room temperature has shown to be tremendously effective at suppressing

physical aging results[20, 21]. Knowledge of why this technique is effective can help shape future storage techniques.

Finally, an aim of this thesis is to begin to explain certain trends in permeability in relation to variation in upstream pressure. It has been documented previously that increasing the feed pressure does not significantly lower the permeability as is expected for materials characterized by a sole Langmuir environment[18]. This result, published by Zhang et al., is interesting and has suggested that there are features of CMS membranes or CMS membrane gas transport that have not been discussed before. Laying the groundwork for future researchers to expand on these initial steps is key.

1.4 Thesis Organization

This work is divided into six chapters, with additional appendices following. Chapter 2 provides the necessary background and theory of transport of penetrants in membranes as well as information regarding CMS formation and structure. Chapter 3 outlines the key materials and methods used in this work, noting any variations of previously published standard operating procedures. Chapter 4 describes a proposed mechanism for physical aging in CMS membranes, as well as key evidence leading to that conclusion. Additionally, it provides several techniques capable of reducing physical aging effects in CMS membranes and relates these findings to the new aging mechanism. Chapter 5 outlines a possible new way to envision transport in CMS membranes, with evidence of CMS membranes exhibiting dual-mode behavior in what has been treated previously as a solely Langmuir material. The envisioned formation mechanism of these two modes is also described. Chapter 6 summarizes the major takeaways from Chapters 4-5 and discusses the implications of both in a unifying way in an attempt to create a self-

consistent model of CMS membranes. Additionally, future work that can shed light on the hypotheses presented is also discussed.

1.5 References

1. Mobil E. 2019 Outlook for Energy: A Perspective to 2040. 2019.

2. Laboratory ORN. Materials for Separation Technologies: Energy and Emission Reduction Opportunities. 2005.

3. Lin H, White LS, Lokhandwala K, Baker RW. Natural gas purification. *Encyclopedia of Membrane Science and Technology* 2013**:** 1-25.

4. The National Academies of Sciences E, and Medicine. A Research Agenda for Transforming Separation Science. 2019.

5. Sholl DS, Lively RP. Seven chemical separations to change the world. *Nature* 2016, **532**(7600)**:** 435-437.

6. Energy USDo. Annual Energy Outlook 2020 with projections to 2050. 2020.

7. Koros WJ. Evolving beyond the thermal age of separation processes: membranes can lead the way. *AIChE Journal* 2004, **50**(10)**:** 2326-2334.

8. Koros WJ, Lively RP. Water and beyond: Expanding the spectrum of large-scale energy efficient separation processes. *AIChE journal* 2012, **58**(9)**:** 2624-2633.

9. Baker RW, Low BT. Gas separation membrane materials: a perspective. *Macromolecules* 2014, **47**(20)**:** 6999-7013.

10. Baker RW, Lokhandwala K. Natural gas processing with membranes: an overview. *Industrial & Engineering Chemistry Research* 2008, **47**(7)**:** 2109-2121.

11. Robeson LM. Correlation of separation factor versus permeability for polymeric membranes. *Journal of membrane science* 1991, **62**(2)**:** 165-185.

12. Robeson LM. The upper bound revisited. *Journal of membrane science* 2008, **320**(1-2)**:** 390-400.

13. Galizia M, Chi WS, Smith ZP, Merkel TC, Baker RW, Freeman BD. 50th anniversary perspective: polymers and mixed matrix membranes for gas and vapor

separation: a review and prospective opportunities. *Macromolecules* 2017, **50**(20)**:** 7809-7843.

14. Ismail AF, Lorna W. Penetrant-induced plasticization phenomenon in glassy polymers for gas separation membrane. *Separation and purification technology* 2002, **27**(3)**:** 173-194.

15. Salinas O, Ma X, Litwiller E, Pinnau I. High-performance carbon molecular sieve membranes for ethylene/ethane separation derived from an intrinsically microporous polyimide. *Journal of Membrane Science* 2016, **500:** 115-123.

16. Rungta M, Wenz GB, Zhang C, Xu L, Qiu W, Adams JS, *et al.* Carbon molecular sieve structure development and membrane performance relationships. *Carbon* 2017, **115:** 237-248.

17. Ma X, Lin Y, Wei X, Kniep J. Ultrathin carbon molecular sieve membrane for propylene/propane separation. *AIChE Journal* 2016, **62**(2)**:** 491-499.

18. Zhang C, Wenz GB, Williams PJ, Mayne JM, Liu G, Koros WJ. Purification of aggressive supercritical natural gas using carbon molecular sieve hollow fiber membranes. *Industrial & Engineering Chemistry Research* 2017, **56**(37)**:** 10482-10490.

19. Adewole J, Ahmad A, Ismail S, Leo C. Current challenges in membrane separation of CO2 from natural gas: A review. *International Journal of Greenhouse Gas Control* 2013, **17:** 46-65.

20. Wenz GB. Tuning carbon molecular sieve membrane performance for challenging gas separations. Georgia Institute of Technology, 2017.

21. Sanyal O, Zhang C, Wenz GB, Fu S, Bhuwania N, Xu L, *et al.* Next generation membranes—using tailored carbon. *Carbon* 2018, **127:** 688-698.

CHAPTER 2

THEORY AND BACKGROUND

2.1 Overview

This chapter will focus on establishing the governing theories of the work presented in later chapters. Transport fundamentals in membranes will first be reviewed, including permeation, sorption and diffusion basics. With this general model in place, transport specifics and its relationship with the currently accepted CMS structure will be discussed.

2.2 Gas Transport in Membranes

In general, a membrane simply acts as a selective barrier, hindering thermodynamic equilibrium from being reached between two separate phases. Assuming the solution-diffusion model, the difference in chemical potential between these two phases causes flux across the membrane, creating a gradient of chemical potential and concentration throughout the selective skin. While a gradient of chemical potential and concentration exist, the entire membrane is assumed to operate at the hydrostatic pressure of the upstream[1]. This concept is summarized in Figure 2.1. Here, variables with the subscript "2" indicate upstream conditions, while the subscript "1" indicates downstream conditions. Broadly, molecules are envisioned to make a series of diffusive jumps through the membrane to various sorption sites, eventually desorbing at the downstream. The differences in flux across the membrane between the two penetrants purifies the feed, as one constituent is inherently "faster."

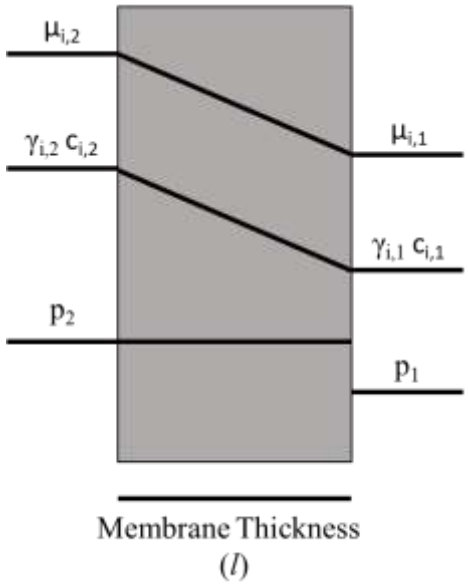

Figure 2.1. Summary of the solution-diffusion model assumptions.

2.2.1 Permeation

Permeability is the fugacity and membrane thickness normalized flux of a specific penetrant, expressed in Equation 2.1.

$$\mathbb{P}_i = \frac{N_i\, l}{\Delta f_i} = \bar{\mathbb{S}}_i\, \bar{D}_i \tag{2.1}$$

Here, $\mathbb{P}_i$ is the permeability of species *i*, N_i is the flux of component *i* through a membrane of thickness *l*, and Δf_i is the fugacity difference of *i* across the membrane. Assuming the solution-diffusion model, $\mathbb{P}_i$ is also equal to the product of the average sorption coefficient, ($\bar{\mathbb{S}}_i$), and average diffusion coefficient, ($\bar{\mathrm{D}}_i$). Often, it is quite difficult to accurately determine the skin thickness, *l*, such as in an asymmetric hollow fiber, which is the focus

of this thesis. In such a case, permeance, a fugacity normalized flux, is used in place of permeability, expressed in Equation 2.2.

$$\frac{\mathbb{P}_i}{l} = \frac{N_i}{\Delta f_i} = \frac{\bar{\mathbb{S}}_i \, \bar{D}_i}{l} \tag{2.2}$$

The selectivity of the membrane for two components is the ratio of each component's permeability or permeance, as in Equation 2.3.

$$\alpha_{i/j} = \frac{\mathbb{P}_i}{\mathbb{P}_j} = \frac{\bar{\mathbb{S}}_i \, \bar{D}_i}{\bar{\mathbb{S}}_j \, \bar{D}_j} \tag{2.3}$$

Permeability is often expressed in the units of Barrer, while permeance is typically expressed in gas permeation units (GPU). GPU is used most frequently in this thesis.

$$1 \, Barrer = \, 10^{-10} \, \frac{cm^3(STP) \, cm}{cm^2 \, s \, cmHg} = 0.33 \, x \, 10^{-15} \frac{mol \, m}{m^2 \, s \, Pa}$$

$$1 \, GPU = \, 10^{-6} \, \frac{cm^3(STP)}{cm^2 \, s \, cmHg} = 3.35 \, x \, 10^{-10} \frac{mol}{m^2 \, s \, Pa}$$

2.2.2 Sorption

$\mathbb{S}_i$ can be described as the concentration of species *i* sorbed at equilibrium in the membrane at a particular fugacity f_i. This can be summarized by Equation 2.4.

$$\mathbb{S}_i = \frac{C_i}{f_i} \tag{2.4}$$

As mentioned in Section 2.2.1, an average sorption coefficient, ($\bar{\mathbb{S}}_i$), is often considered in place of local sorption coefficients. $\bar{\mathbb{S}}_i$ is defined in Equation 2.5.

$$\bar{\mathbb{S}}_i = \frac{C_{i,2} - \, C_{i,1}}{f_{i,2} - \, f_{i,1}} \tag{2.5}$$

The specific equation describing concentration is dependent on the class of membrane being used. Sorption in glassy polymers is described by dual-mode sorption, where penetrants have access to a mode characterized by Henry's law sorption, and a mode characterized by Langmuir sorption[2]. This idea is expressed in Equation 2.6

$$C_i = C_{D,i} + C_{H,i} \tag{2.6}$$

Here, $C_{D,i}$ denotes the concentration of species *i* in the "dissolved" mode and $C_{H,i}$ denotes the concentration of species *i* sorbed in "holes." The equation describing concentration within each mode is shown in Equation 2.7-2.8:

$$C_{D,i} = k_{D,i} f_i \tag{2.7}$$

$$C_{H,i} = \frac{C'_{H,i} b_i f_i}{1 + b_i f_i} \tag{2.8}$$

where $k_{D,i}$ is the Henry's coefficient, $C'_{H,i}$ is the Langmuir hole-filling capacity, and b_i is the Langmuir affinity constant of species *i* in that particular membrane. The equation for $C_{H,i}$ can easily be corrected to accommodate a combination of different species, such as a binary mixture of penetrants[3]. This is shown in Equation 2.9

$$C_{H,i} = \frac{C'_{H,i} b_i f_i}{1 + b_i f_i + b_j f_j} \tag{2.9}$$

Because CMS membranes are rigid sieves, sorbed concentration in CMS has been described by a Langmuir isotherm, meaning concentration in CMS can be defined as shown in Equation 2.10 [4, 5].

$$C_i = C_{H,i} = \frac{C'_{H,i} b_i f_i}{1 + b_i f_i + b_j f_j} \tag{2.10}$$

2.2.3 Diffusion

Diffusion in both glassy polymer and CMS membranes is an activated process, where the penetrant must reach a certain energetic and entropic threshold to make a diffusive jump. This can be described by an Arrhenius relationship shown in Equation 2.11 [6].

$$D_i = D_{i,0} e^{\frac{-E_{D,i}}{RT}} \tag{2.11}$$

Diffusion of penetrants can also be analogized to the Eyring theory of rate processes, shown in Equation 2.12 [7].

$$D_i = \lambda^2 \frac{k_B T}{h} e^{S_{D,i}/R} e^{-H_{D,i}/RT} \tag{2.12}$$

Here, λ is the average diffusive jump length, $\frac{k_B T}{h}$ is the frequency of vibration in the activated state, and S_D and H_D represent the activation entropy and enthalpy, respectively. The activation enthalpy can be simplified assuming negligible volume change to produce a form of Equation 2.12 that resembles 2.11. This is highlighted in Equations 2.13 and 2.14.

$$H_D = E_D + PV = E_D + RT \tag{2.13}$$

Inserting this into Equation 2.12, Equation 2.14 is derived.

$$D_i = e\lambda^2 \frac{k_B T}{h} e^{S_{D,i}/R} e^{-E_{D,i}/RT} \tag{2.14}$$

Although the diffusion process is governed by similar equations in both flexible glassy polymer and more rigid CMS membranes, the physical interpretations of such processes is quite different. This is best illustrated by Figure 2.2. In glassy polymers, movements of

the polymer chains are envisioned to create space for the penetrant to jump. In rigid sieves, penetrants make diffusive jumps through a permanent microporosity, forming an activated complex in the sieving site.

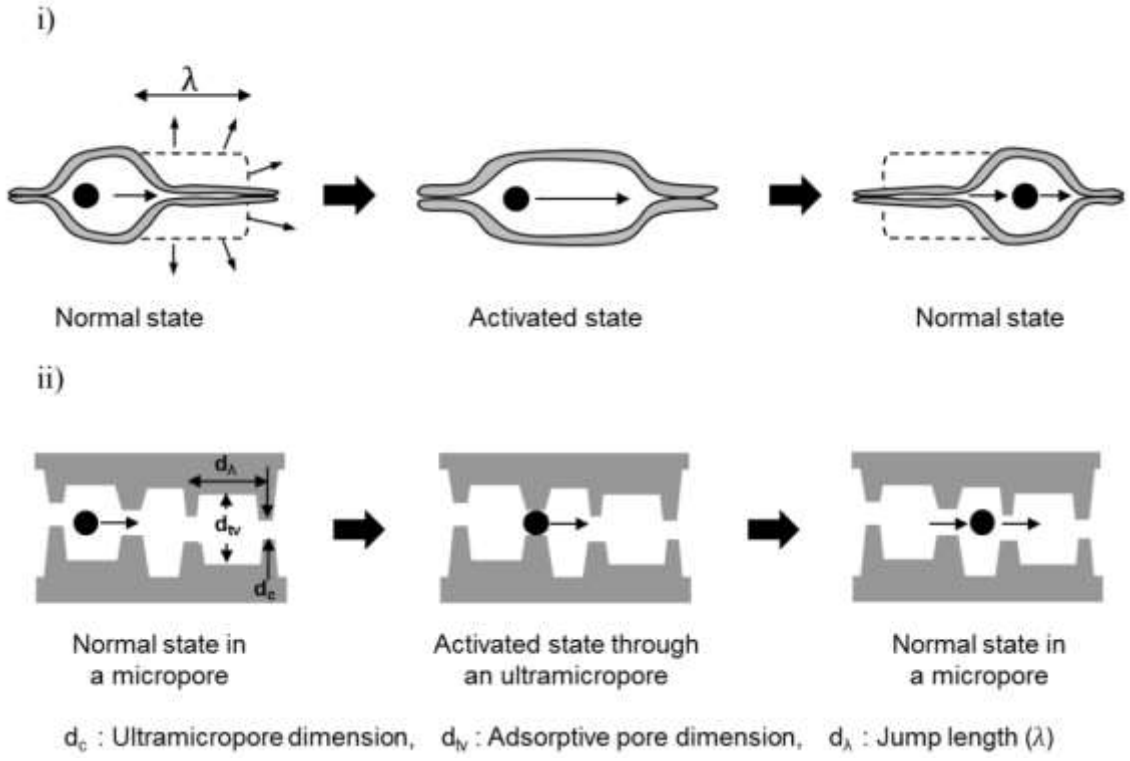

Figure 2.2. Envisioned activated transport through i) flexible polymer membranes, and ii) rigid CMS membranes [8].

2.3 Formation and Structure of Carbon Molecular Sieves

This section will discuss the published formation mechanism first proposed by Rungta & Wenz et al[9]. Chapter 4 and 5 will discuss refinements to the mechanism, but the basic structure must be established first. A key trait of CMS membranes is their exceptional combination of high permeability and high selectivity[10]. This is even more interesting considering transport properties of the polymer precursor, such as sorption capacity and diffusion selectivity, are significantly lower than the CMS membrane[11]. Therefore, the formation mechanism must provide a pathway from flexible polymer coils to rigid molecular sieves.

Rungta & Wenz proposed a four-step process that occurs during pyrolysis of the glassy polymer precursor. The pyrolysis protocol can be summarized in Figure 2.3. During the temperature ramp, the entangled polymer is envisioned to experience significant stresses as it attempts to straighten out during aromatization, causing it to fragment at weak links. Supported by Adams & Itta et al., the fragments aromatize, forming strands[12]. Interestingly, what Adams & Itta showed is that, for CMS derived from 6F precursors, two strand types form: a pyrrolic strand and a pyridinic strand, shown in Figure 2.4. By examining ratio of CO and CO_2 removed during the pyrolysis process, insight can be drawn on the ratio of pyrrolic strands to pyridinic strands, respectively[12].

With this collection of pyrrolic and pyridinic strands, the strands are believed to attempt to organize into plate-like structures to accommodate limited available free volume. This transition from randomly oriented aromatic structures to organized collections with similar orientation resembles the isotropic-to-nematic phase transition in liquid crystals. Here, there is an entropic benefit for the strands to arrange themselves into

plates, as doing so increases translational freedom, even if rotational freedom is sacrificed in the process[13, 14]. This interesting, seemingly counterintuitive step during the CMS formation process forms the plates that provide the high permselectivity characteristic of CMS membranes. Small slits, termed ultramicropores, between the aromatic strands within a plate provide the ideal size for molecular sieving, capable of discriminating between different rotational degrees of freedom of certain gas pairs[15, 16].

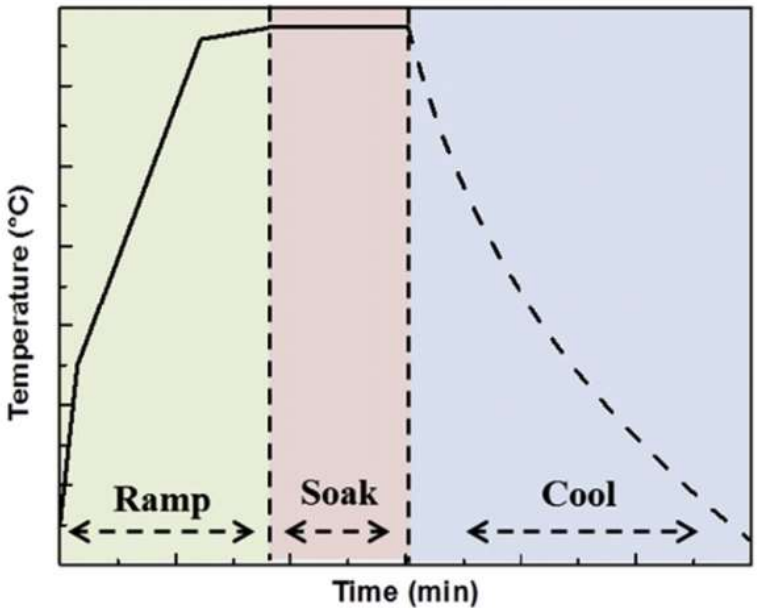

Figure 2.3. Steps of a typical CMS pyrolysis protocol[9].

As the ultramicroporous plates develop, packing voids are envisioned to form between them due to imperfect arrangement of the plates. These voids, termed micropores,

provide favorable sorption sites, essentially limited to the number of sorbates required to fill the voids, explaining the large Langmuir capacity seen in CMS sorption isotherms[17, 18].

During the high temperature soak and cooling steps of the pyrolysis, the micropores and ultramicropores are believed to become more perfect, "healing" defects in the structure, eventually forming a complex distribution of microporous cells with ultramicroporous walls. Different ramp, soak, and cooling rates are believed to change the CMS structure, as different times within each step should change the fragments, plates, and the level of perfection in the CMS structure. The pyrolysis process as a whole can be summarized by Figure 2.5.

a)

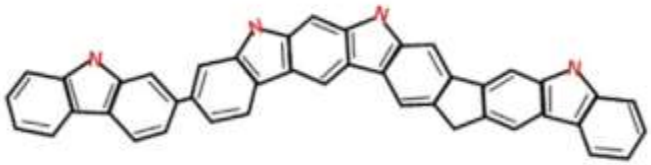

b)

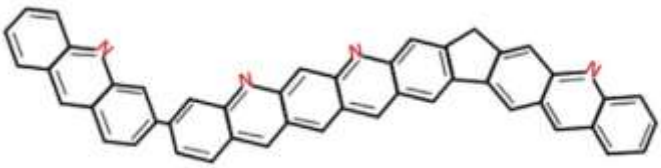

Figure 2.4. Envisioned a) pyrrolic and b) pyridinic strands in CMS membranes[12].

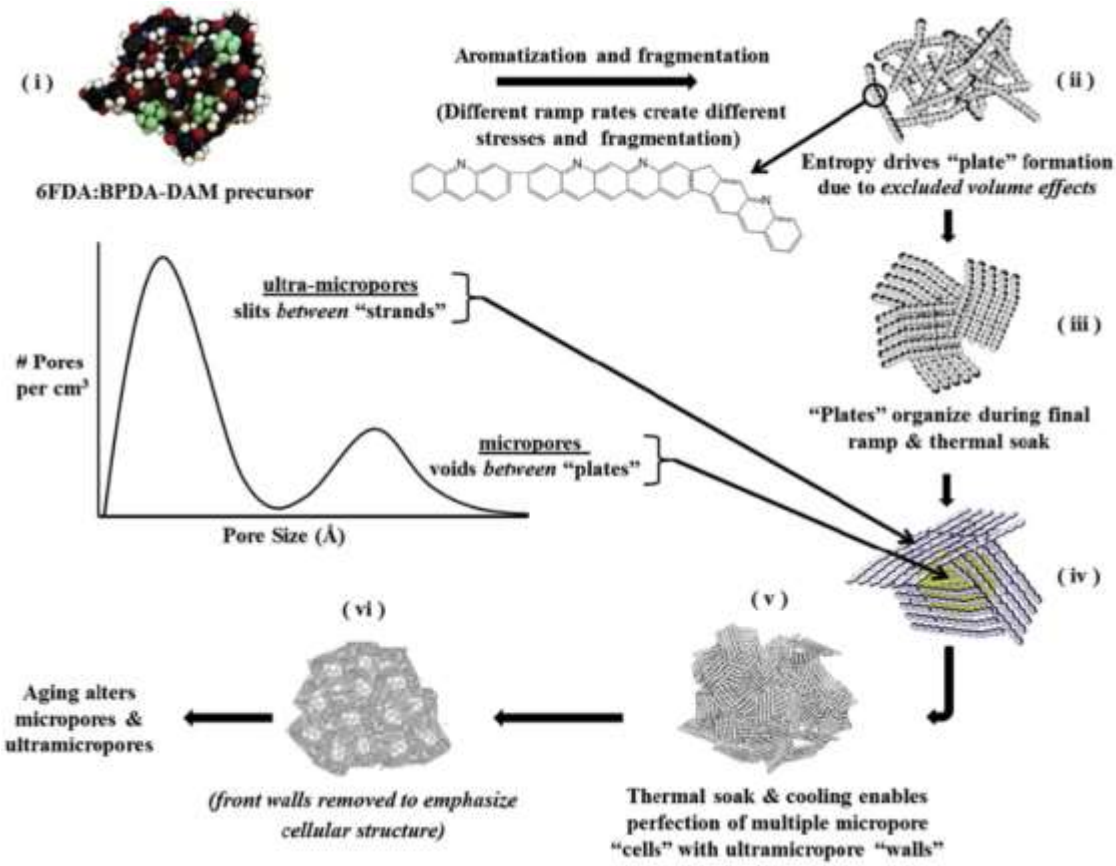

Figure 2.5. Envisioned CMS formation process from flexible glassy polymer to rigid CMS membrane[9].

It is important to note additional structural differences between asymmetric hollow fiber membranes and dense film membranes, as this difference features into Chapter 4. The asymmetric CMS hollow fiber membranes used in this work consisted of two distinct layers: a dense selective skin and a porous substructure. The dense selective skin contains the micropores and the ultramicropores, and thus is the region where the actual separation occurs. The porous substructure contains significantly larger pores, and as its name suggests, merely acts as structural support for the dense skin. There is still sorption in this portion of the membrane, however the corresponding diffusion coefficient is believed to be orders of magnitudes larger than diffusion coefficients in the dense skin. A CMS dense film membrane only consists of the selective region, meaning there is no porous substructure.

2.4 References

1. Wijmans JG, Baker RW. The solution-diffusion model: a review. *Journal of Membrane Science* 1995, **107**(1)**:** 1-21.

2. Paul DR, Koros W. Effect of partially immobilizing sorption on permeability and the diffusion time lag. *Journal of Polymer science: Polymer physics edition* 1976, **14**(4)**:** 675-685.

3. Langmuir I. A new adsorption isotherm. *J Am Chem Soc* 1918, **40:** 1361-1403.

4. Koros WJ, Chern RT, Stannett V, Hopfenberg HB. A model for permeation of mixed gases and vapors in glassy polymers. *Journal of Polymer Science: Polymer Physics Edition* 1981, **19**(10)**:** 1513-1530.

5. Koros W. Model for sorption of mixed gases in glassy polymers. *Journal of Polymer Science: Polymer Physics Edition* 1980, **18**(5)**:** 981-992.

6. Van Amerongen GJ. The permeability of different rubbers to gases and its relation to diffusivity and solubility. *Journal of Applied Physics* 1946, **17**(11)**:** 972-985.

7. Glasstone S, Laidler KJ, Eyring H. *The theory of rate processes*. McGraw-hill, 1941.

8. Rungta M. Carbon molecular sieve dense film membranes for ethylene/ethane separations. Georgia Institute of Technology, 2012.

9. Rungta M, Wenz GB, Zhang C, Xu L, Qiu W, Adams JS, *et al.* Carbon molecular sieve structure development and membrane performance relationships. *Carbon* 2017, **115:** 237-248.

10. Sanyal O, Zhang C, Wenz GB, Fu S, Bhuwania N, Xu L, *et al.* Next generation membranes—using tailored carbon. *Carbon* 2018, **127:** 688-698.

11. Ning X, Koros WJ. Carbon molecular sieve membranes derived from Matrimid® polyimide for nitrogen/methane separation. *Carbon* 2014, **66:** 511-522.

12. Adams JS, Itta AK, Zhang C, Wenz GB, Sanyal O, Koros WJ. New insights into structural evolution in carbon molecular sieve membranes during pyrolysis. *Carbon* 2019, **141:** 238-246.

13. Flory PJ. Molecular theory of liquid crystals. *Liquid Crystal Polymers I*. Springer, 1984, pp 1-36.

14. Gelbart WM. Molecular theory of nematic liquid crystals. *The Journal of Physical Chemistry* 1982, **86**(22)**:** 4298-4307.

15. Singh A, Koros W. Significance of entropic selectivity for advanced gas separation membranes. *Industrial & engineering chemistry research* 1996, **35**(4)**:** 1231-1234.

16. Fu S, Sanders ES, Kulkarni S, Chu Y-H, Wenz GB, Koros WJ. The significance of entropic selectivity in carbon molecular sieve membranes derived from 6FDA/DETDA: DABA (3: 2) polyimide. *Journal of Membrane Science* 2017, **539:** 329-343.

17. Fu S, Sanders ES, Kulkarni SS, Koros WJ. Carbon molecular sieve membrane structure–property relationships for four novel 6FDA based polyimide precursors. *Journal of Membrane Science* 2015, **487:** 60-73.

18. Fu S, Sanders ES, Kulkarni SS, Wenz GB, Koros WJ. Temperature dependence of gas transport and sorption in carbon molecular sieve membranes derived from four 6FDA based polyimides: Entropic selectivity evaluation. *Carbon* 2015, **95:** 995-1006.

CHAPTER 3

MATERIALS AND EXPERIMENTAL METHODS

3.1 Overview

This chapter will describe the materials and experimental methods used in Chapters 4 and 5. Standard operating procedures for CMS dense films and hollow fibers are discussed. Additionally, several revisions to existing standard procedures have been made to study the physical aging process. These revisions have been addressed below.

3.2 Materials

3.2.1 6FDA:BPDA-DAM polymer hollow fiber membranes

As the title of the thesis suggests, this work focuses specifically on CMS membranes derived from 6FDA:BPDA-DAM (1:1), hereafter referred to as "6F" precursors. For this work, CMS hollow fiber membranes were provided by industrial partners. The structure of the precursor is shown below in Figure 3.1.

3.2.2 Gases

All gases used in this work were either purchased from Airgas or Nexair. All pure and mixed gases except those involving C_3H_6 and C_3H_8 were purchased from Airgas, while C_3H_6 and C_3H_8 were purchased from Nexair. All pure and mixed gas permeation and pure gas sorption experiments were performed with research grade gas, (99.999% purity). CO_2 storage, unless otherwise noted, was performed using industrial grade purity, (99.97%).

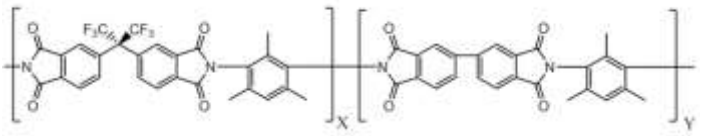

Figure 3.1. Structure of 6FDA:BPDA-DAM (1:1). 6FDA – 4,4' (hexafluoroisopropylidene) diphthalic anhydride. BPDA – 3,3'-4,4'-biphenyl tetracarboxylic dianhydride. DAM – 2, 4, 6-trimethyl-1, 3-phenylene diamine.

3.3 Membrane Formation

3.3.1 6FDA:BPDA-DAM polymer dense film membranes

To allow for proper comparison between CMS hollow fibers and dense films, 6F hollow fibers were dissolved and cast into films whenever films were required. The process used in this work is similar to those discussed in previous theses[1]. Initially, fibers were dried under vacuum at 120 °C overnight. Next, the fibers were dissolved in dichloromethane, (DCM), purchased in sure-seal bottles from Sigma-Aldrich, to create a 3 wt% polymer solution. This solution was then left on rollers for roughly 18 hours to allow for proper dissolution of the polymer, then filtered using 0.2 μm hydrophobic PTFE syringe filters to remove any large impurities. Next, the solution, along with excess DCM reservoirs, was placed in a glove bag. The glove bag was purged with N_2 several times to remove as much air as possible, then sealed off. The glove bag environment was left for 3 hours to allow for significant DCM saturation of the N_2 atmosphere. After this time, the polymer solution was cast onto a Teflon plate, and the plate and solution were covered with a glass dome to slow the DCM evaporation process further, then left for 3 days to allow

the film to vitrify. The film was then dried at 120 °C under vacuum for 24 hours to remove any residual solvent.

3.3.2 Pyrolysis Protocols

All CMS hollow fibers and dense films in this work were pyrolyzed in a three-zone furnace, (model # XST-3-024-3C, Thermcraft Inc., Winston-Salem, NC). A schematic of the furnace setup is shown below in Figure 3.2.

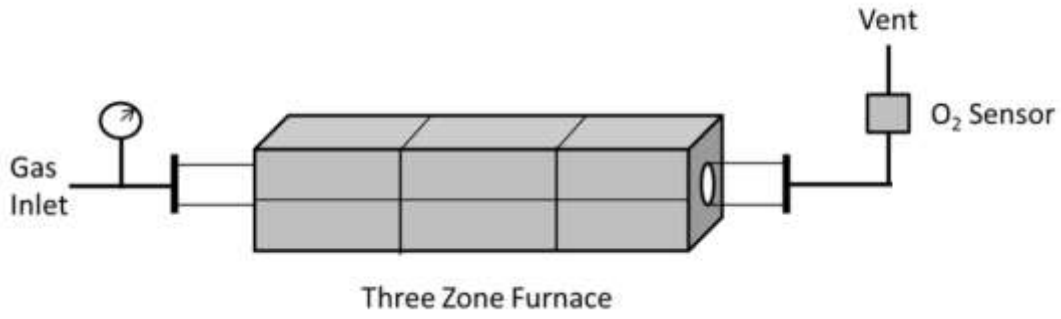

Figure 3.2. Schematic of a typical three-zone pyrolysis setup.

All hollow fibers and dense film precursors were pyrolyzed on a stainless-steel mesh. The CMS pyrolysis protocol used in this work, referred to as the "standard 550 °C protocol," is discussed below. Before any temperature treatment, the system was purged with UHP Argon for at least 8 hours. The pyrolysis was not performed if the oxygen concentration in the system was higher than 1 ppm O_2.

Start – 50 °C

Point 1 – 50 °C to 250 °C in 15 minutes

Point 2 – 250 °C 535 °C in 74 minutes

Point 3 – 535 °C to 550 °C in 60 minutes

Point 4 – 550 °C temperature soak for 120 minutes

Finish – Natural cooling from 550 °C to below 50 °C

Thorough furnace cleaning and burnout protocols were used prior to any pyrolysis. Furnace cleaning is a relatively new practice, outlined in a previous work by Sanyal et al[2]. Before a pyrolysis, the metal fittings comprising the pyrolysis furnace were broken down into their individual Swagelok parts and flanges. These pieces were then placed in n-methyl pyrrolidone, (NMP), and heated to approximately 100 °C for at least 6 hours. The pieces were then cooled and dried before being placed in water and then acetone for 6 hours each. Then they were dried at approximately 200 °C overnight. NMP and acetone were both purchased from Sigma-Aldrich, (St. Louis, MO).

After cleaning, a standard burnout procedure, shown in previous work, was used[3]. Before the actual burnout protocol, both the quartz tube and stainless-steel mesh were rinsed with acetone to remove any visible remnants from previous pyrolyses. The furnace parts, both the ones cleaned with NMP and the quartz tube, were then connected with the stainless-steel mesh sealed inside the furnace. The burnout temperature profile is shown below, performed in a dry air environment.

Start – 50 °C

Point 1 – 50 °C to 900 °C in 90 minutes

Point 2 – 900 °C temperature soak for 480 minutes

Finish – Natural cooling from 900 °C to below 50 °C

For both the burnout and the pyrolysis, the flowrate of the respective gas was maintained with a mass flow meter, (model # MC-500-SCCM-D, Alicat Scientific, Marana, AZ), to be 500 sccm. Studies were not done to check the effect of purge flowrate, but all pyrolysis runs were performed under this condition.

3.4 Membrane Characterization

This section will discuss the protocols used for several experimental techniques. As a major focus of this work was to understand the physical aging process, several revisions have been added to standard operating procedures common with such techniques. However, careful controls were performed to ensure that the operating procedures used still gave valid results.

3.4.1 Permeation

Two permeation techniques were used for this thesis, commonly referred to as constant volume and constant pressure permeation. The constant volume permeation technique was used most frequently, as it allowed for more accurate measurements of flux across the membrane. Additionally, only single fiber modules were used, to ensure changes in permeance and selectivity could be attributed to a specific membrane.

3.4.1.1 Construction of CMS single-fiber modules for Permeation Experiments

Detailed descriptions of the module construction process can be found in a previous publication[4]. All modules were constructed to be roughly 12 cm in effective length. Both ends of a module were sealed around the CMS hollow fiber by packing Teflon tape and then filled with 3M DP-100 epoxy to ensure that the only passage into the shell of the module is through the bore of the CMS fiber, and vice versa. All modules were given roughly 24 hours for the epoxy to cure.

3.4.1.2 Constant Volume Permeation

Constant volume permeation tests allow for measuring of permeance by measuring the changes in pressure over time in a constant, known volume. Additional information on this technique can be found in previous publications[4, 5, 6]. Before the experiment, the system, including the module, was exposed to vacuum for a total of 30 minutes to remove any species from the system that might affect the measurement. Following the vacuum exposure, a leak test was performed on the system. If the measured leak rate was more than 1% of the expected flux, the experiment was not pursued until the leak rate had been lowered to below that threshold. Once the upstream had been pressurized with the intended feed, all permeation experiments were given at least 3 hours to reach a steady state permeance. For mixed-gas permeation tests, the stage-cut was maintained at <1% to reduce the effects of concentration polarization on the surface of the membrane. The composition of the permeate in mixed-gas tests was analyzed using a Bruker 450 gas chromatograph with a Thermal Conductivity Detector. All permeation tests were performed at 35 °C.

3.4.1.3 Constant Pressure Permeation

Long-term permeation tests were performed using the constant pressure permeation technique. Here, the downstream was maintained at a constant pressure, (atmospheric), and the flux across the membrane was measured using a bubble flow meter to calculate volumetric flow rate. Like with the constant volume method, all permeation tests were performed at 35 °C. Mixed gas permeation experiments had a maintained stage-cut of <1%. The same gas chromatograph mentioned in Section 3.4.1.3 was used to analyze permeate compositions. Permeation experiments were given at least 3 hours to reach steady state.

3.4.2 Pressure Decay Sorption

The pressure decay sorption technique was used to measure sorption isotherms for gases and has been described previously[7]. After loading the CMS sample into the sorption system, the sorption cells of known volume, (sample cell and reservoir cell), were evacuated and maintained at vacuum for roughly 3 hours. Next, the valve separating the two cells was closed and the pressure in each cell was monitored for 1 hour. This was performed to check that sample had been significantly degassed. If the change in pressure vs. time was measured to be less than 10^{-6}, the sorption experiment was continued. For each point, the reservoir cell was filled to a desired pressure and allowed to sit for 20 minutes to allow for the gas in the reservoir to reach the isotherm temperature. Following the thermal equilibrium time, the valve separating the cells was opened for 1 second, then closed. The pressures in the cells were then monitored for at least 4 hours to allow the sample to reach equilibrium, and a mass balance was performed to determine the moles

sorbed in the CMS. The next point in the isotherm was only pursued if the change in pressure vs. time of the previous point was less than 10^{-6}.

3.4.3 Automated Gravimetric Sorption

Gravimetric sorption, using a TA VTI-SA+ vapor sorption analyzer (TA Instruments, New Castle, DE), was used to measure the isotherms of n-pentane, n-hexane, and water in CMS membranes. Before the sorption isotherms were obtained, a calibration of the system was performed using water and sodium chloride. Once properly calibrated, the crushed CMS hollow fiber membranes were placed in a glass container attached to a spring. The sorption of the hydrocarbons was measured from an activity of 0.1 to 0.7, while water was measured from 0.05 to 0.90, all at 25 °C. For each isotherm, (n-pentane, n-hexane, and water), a sensitivity threshold limit of 0.0005% for 30 minutes was used, meaning if the mass of the sample of the spring changed by less than 0.0005% in a 30 minute window, the system automatically changed to the next scheduled activity.

3.4.4 Complementary Characterization Techniques

3.4.4.1 BET Measurements

CO_2 physisorption was used to measure the surface area of CMS hollow fiber membranes before and after aging using Micromeritics ASAP 2020. These experiments were carried out at 0 °C with a pressure range of 3 mmHg to 1 atmosphere. After the initial surface area measurement, the sample was aged under vacuum for 1 week, then the surface area was remeasured using the same conditions.

3.4.4.2 Raman Spectroscopy

Raman spectroscopy was performed on CMS dense film samples. Like the physisorption measurements, samples were aged for 1 week under vacuum after initial measurements in an attempt to produce any measurable change to the CMS structure. Renishaw Raman Spectroscopy was used to perform the measurements. Samples were examined with a 50X magnification lens. A 488 nm laser was used with 1% laser power, 10 seconds of exposure, and 2 accumulations. Both single-point and mapping measurements were performed to measure various regions of the CMS dense film.

3.4.4.3 X-Ray Diffraction

CMS dense films were used to measure x-ray diffraction with a PANalytical Empyrean XRD machine. All samples were placed on a zero-background plate. The diffraction was measured from $2\Theta = 1° - 70°$. Like the previous two characterization techniques, x-ray diffraction was measured both on fresh films and films aged 1 week under vacuum.

3.5 Miscellaneous Techniques

Some techniques used in this work do not classify as membrane characterization, although are necessary for proper replication of experiments. These are described here.

3.5.1 CMS Hollow Fiber Storage

A key portion of this thesis is centered on the effect of different storage conditions on CMS aging rates. To store CMS hollow fiber modules, a feed line is attached to the bore of the module and pressurized to the intended storage pressure. Importantly, all remaining sides of the module, (two shell side connections and 1 additional bore side connection), are left open to allow for a purging of any remaining penetrants from previous

permeation experiments. The module is left in this condition for 10 minutes. Next, the remaining bore side is closed, leaving only the two shell side connections open. The module is now left this way for 20-30 minutes to allow for the storage penetrant to start permeating through the skin. After the 20-30 minutes, the two shell side connections are capped, and the module is left this way for the remainder of the storage period.

3.5.2 CMS Regeneration using C_3H_6 and C_3H_8

Chapter 4 will discuss the effects of regeneration on CMS membranes. This technique, first described by Jones & Koros, is very similar to CMS storage described above[8]. The same capping procedure is performed to remove as many sorbed penetrants from permeation experiments as possible. In this case, however, there is simply higher activity gas being used as the storage medium. After the capping procedure is performed, the module is left in this condition for 72 hours to allow for the entire skin to saturate with the storage medium. After the storage period, the pressure is released rather quickly. It is unknown if the speed of disconnection is important for the effectiveness of the regeneration technique, as optimization studies were not performed. If done correctly, evaporation of C_3H_6 or C_3H_8 should be observed as the module is disconnected from the storage system. An important variable to consider when performing this technique is temperature. According to Jones, high activity is required for this regeneration technique to occur. If this is correct, the temperature of the environment holding the gas cylinder must be monitored. Small changes in temperature, (2-3 °C), can significantly change the vapor pressure of the respective storage medium, and thus significantly change the activity. It is helpful to have a thermometer close to the cylinder to allow for easy adjustments of pressure to accommodate temperature changes.

3.6 References

1. Wenz GB. Tuning carbon molecular sieve membrane performance for challenging gas separations. Georgia Institute of Technology, 2017.

2. Sanyal O, Hicks ST, Bhuwania N, Hays S, Kamath MG, Karwa S, *et al.* Cause and effects of hyperskin features on carbon molecular sieve (CMS) membranes. *Journal of Membrane Science* 2018, **551:** 113-122.

3. Hays SS, Sanyal O, León NE, Arab P, Koros WJ. Envisioned role of slit bypass pores in physical aging of carbon molecular sieve membranes. *Carbon* 2020, **157:** 385-394.

4. Vu DQ, Koros WJ, Miller SJ. High pressure CO2/CH4 separation using carbon molecular sieve hollow fiber membranes. *Industrial & engineering chemistry research* 2002, **41**(3)**:** 367-380.

5. Pye D, Hoehn H, Panar M. Measurement of gas permeability of polymers. I. Permeabilities in constant volume/variable pressure apparatus. *Journal of Applied Polymer Science* 1976, **20**(7)**:** 1921-1931.

6. Pye D, Hoehn H, Panar M. Measurement of gas permeability of polymers. II. Apparatus for determination of permeabilities of mixed gases and vapors. *Journal of applied polymer science* 1976, **20**(2)**:** 287-301.

7. Koros WJ, Paul D. Design considerations for measurement of gas sorption in polymers by pressure decay. *Journal of Polymer Science: Polymer Physics Edition* 1976, **14**(10)**:** 1903-1907.

8. Jones CW, Koros WJ. Carbon molecular sieve gas separation membranes-II. Regeneration following organic exposure. *Carbon* 1994, **32**(8)**:** 1427-1432.

CHAPTER 4

PHYSICAL AGING IN CARBON MOLECULAR SIEVE MEMBRANES

4.1 Overview

This chapter will focus on the physical aging mechanism in 6FDA:BPDA-DAM CMS membranes. Membrane stability has been listed as a key feature needed for commercial application of developing membrane technology[1, 2], so having a detailed understanding of the structural changes occurring in CMS membranes is necessary for development of tools and techniques to minimize physical aging effects. This chapter provides both a connection between physical features of CMS membranes and their effects on transport properties.

Additionally, this chapter provides several different techniques capable of both suppressing the rate of physical aging during membrane storage as well as some capable of regenerating already-aged CMS membrane samples. The findings presented in this chapter may seem to contradict previous work examining the physical aging mechanism[3]. However, it is important to note the mechanism proposed here and proposed previously are not mutually exclusive. Both can coexist within the CMS membrane class of materials, where the one proposed here becomes apparent over a shorter period of time and thus plays more of a role in observed permeation changes.

It is also vital to note that there are distinct differences between physical aging in CMS membranes vs. glassy polymer membranes. Although transport changes appear very similar (e.g. drop in permeability, increase in permselectivity, self-retarding aging rate,

etc.), the mechanisms and forces controlling the mechanisms are not. The differences between the two mechanism will be clear as the chapter continues.

4.2 Physical Aging of Carbon Molecular Sieve Membranes under Pentane, Hexane, and Water Environments

Xu et al. first proposed that CMS membranes can be treated as a complex glass when explaining the physical aging mechanism[3]. Their work showed that over long periods of time the sorption capacity of the CMS decreases, resembling the glassy polymer aging mechanism which can be briefly described as *diffusion of free volume*[4, 5, 6, 7]. Essentially, Xu et al. noted that there appears to be unrelaxed free volume, and the decrease in permeability can be attributed to the membrane rearranging itself to pack more closely, eliminating that free volume.

Using this mechanism, it was proposed to begin the work for this thesis that saturating the micropores in CMS membranes could minimize the physical aging effect, illustrated generally in Figure 4.1. If the plates in the membrane cannot pack, then physical aging should be restricted. (This will be shown not to be the case in the coming sections). Ideally, this would be done with a very low-pressure storage medium to allow for lower pressurization of modules containing thousands of CMS fibers. This intuitively suggests using larger hydrocarbons, such as pentane and hexane. These molecules also have the added benefit of being of good size to "prop" open a micropore structure. From previous N_2 and CO_2 physisorption data on 550 °C UHP Ar CMS membranes derived from 6FDA:BPDA-DAM, a range of ultramicropore and micropore sizes was obtained; the measurable ultramicropores range from 4-7 Å , and the micropores range from 7-20 Å[8].

Pentane and hexane have ideal size for this type of pore distribution, as shown in Table 4.1. Both molecules are able to fit through the tight ultramicropores but are still able to quickly saturate the micropores due to their large length dimension.

Figure 4.1. Schematic illustrating CMS storage under large organics illustrated in green. After the intended storage period, the dimensions of the micropore, "d", is hypothesized to be the same due to molecular "pillars," meaning $d_i = d_f$.

Additionally, water, being incredibly safe and easily accessible, would be an ideal storage medium. As a first trial, these three molecules (pentane, hexane, and water), were selected as possible ideal storage media to minimize physical aging effects of CMS membranes.

Table 4.1. Dimensions of molecules used for low-pressure CMS membrane storage. Dimensions of n-pentane and n-hexane were taken from an outside source[9].

Molecule	Length Å	Width Å	Height Å
n-Pentane	9.315	4.154	4.846
n-Hexane	10.617	4.154	4.846

4.2.1 Sorption Isotherms of Pentane, Hexane, and Water in Carbon Molecular Sieve Membranes

As mentioned above, it was hypothesized that saturated micropores cannot age because movement of CMS plates is more restricted. Therefore, in order to properly test this hypothesis, the CMS saturation condition for each respective molecule type must be known. These were obtained by using gravimetric sorption outlined in Section 3.4.3. The sorption isotherms for pentane, hexane, and water are shown in Figure 4.2 a-c. As expected, due to the organophilic tendencies of CMS membranes, the membrane is saturated with both pentane and hexane at very low molecule activities. The sorption isotherm for water also is intuitive.

a)

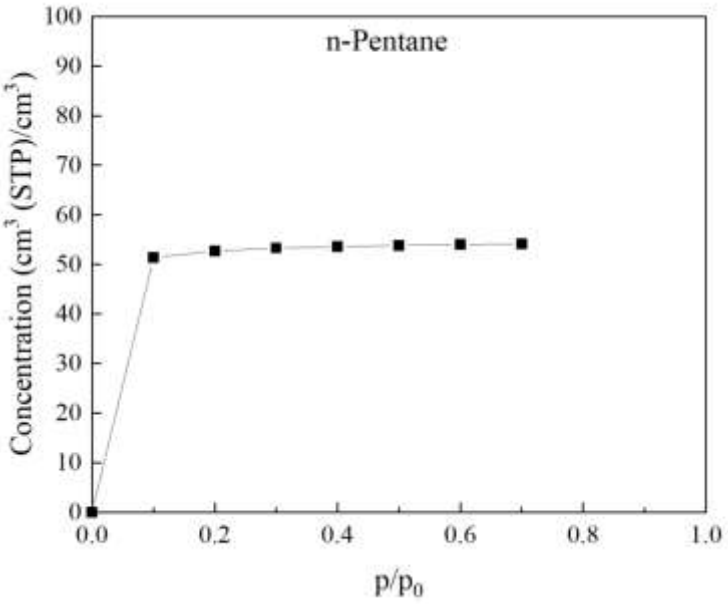

b)

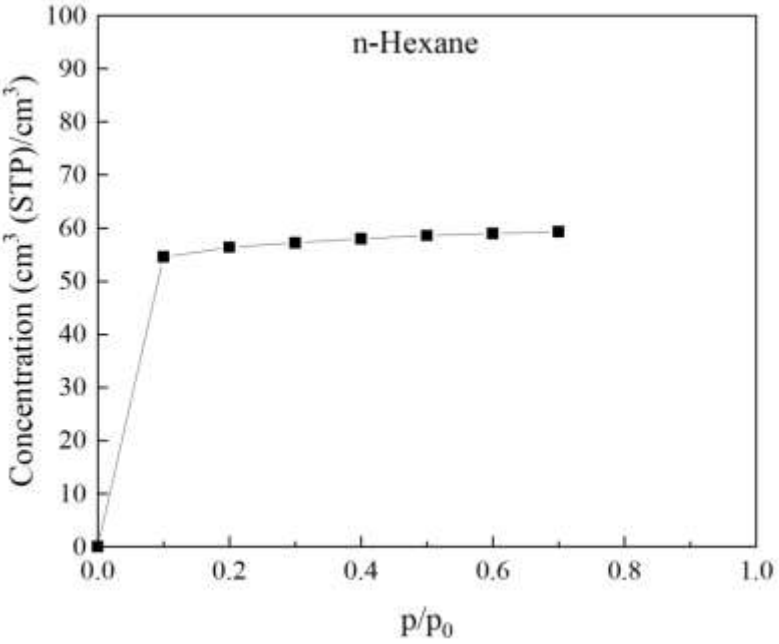

c)

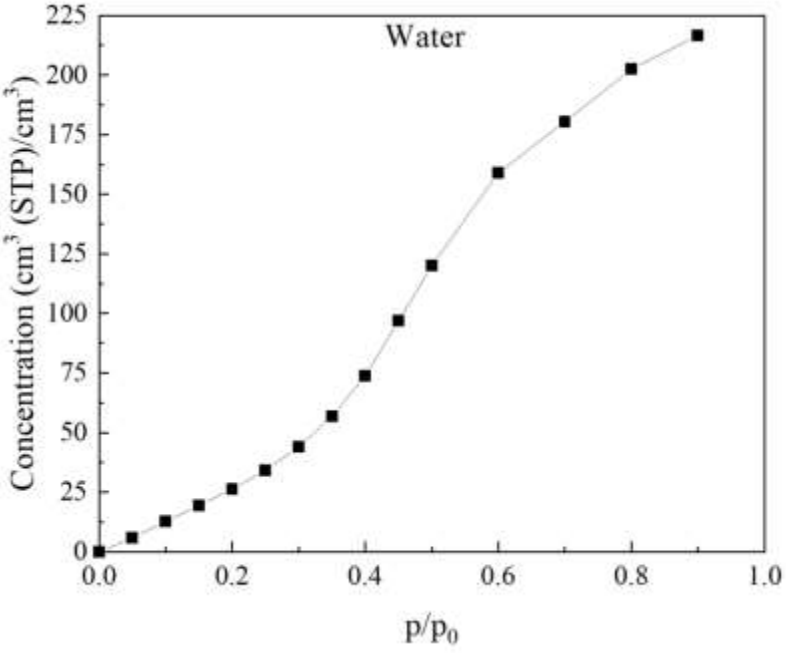

Figure 4.2. Sorption of 6F-derived 550 °C UHP Ar CMS hollow fibers at 25 °C for a) n-pentane, b) n-hexane, and c) water.

At low p/p_0, the CMS environment is unfavorable for water molecules, as CMS is so organophilic. However, once p/p_0 reaches roughly 0.5, hydrophilic interactions between water molecules begin to become more prominent, creating a much more favorable environment for additional water molecules to sorb. Figure 4.2c suggests that, for CMS to saturate with water, a very high value of p/p_0 is required.

4.2.2 Regeneration of Carbon Molecular Sieve Membranes Exposed to Pentane, Hexane, and Water

A good storage medium to minimize physical aging effects is one that is easily sorbed in the CMS, one that is easily removed from the CMS, and one that effectively minimizes the aging phenomena. Section 4.2.1 established the ease of saturating the CMS with each respective proposed storage medium. This section will focus on removal of the storage media.

Cheryl Jones demonstrated the difficulty of removing large organic contaminants once sorbed in CMS[10, 11]. Importantly, her work also established a technique capable of removing these contaminants. By exposing the contaminated membrane to high activity C_3H_6 for an extended period of time, significant restoration of O_2 flux was observed. The flux had been essentially zero after initial contaminant exposure.

This technique provides a relatively simple method to remove the sorbed pentane, hexane, and water. To test the effectiveness of C_3H_6 regeneration for these cases, first a permeance baseline was established on several modules. Following completion of the baseline test, the individual modules were exposed to the storage media in their respective way. For the organic compounds, 50 psia N_2 was bubbled through either liquid pentane or

liquid hexane and carried into the bore side of the membrane for 24 hours. The shell side was capped to allow for significant saturation to build up across the majority of the membrane skin. For water storage, CMS fibers were soaked in liquid water for 24 hours before module making, and the baseline was taken to be the average of the baselines for pentane and hexane.

Following the 24-hour exposure time, helium flux was measured across the membranes to ensure complete membrane shut down from contaminant exposure. In all cases, no helium flux was observed. After confirming membrane shut down, following the method proposed by Jones & Koros[10], the modules were exposed to an upstream pressure of 100 psia dry air, while the downstream was maintained at 1 atmosphere, again for 24 hours. Finally, the modules were treated using C_3H_6. Here, high activity C_3H_6 (>95% unit activity), was exposed to the bore side of the membrane at room temperature, while the shell side was capped, for 72 hours. Following the storage period, the modules were depressurized and tested again. The results from this study are shown in Figure 4.3 a-c.

a)

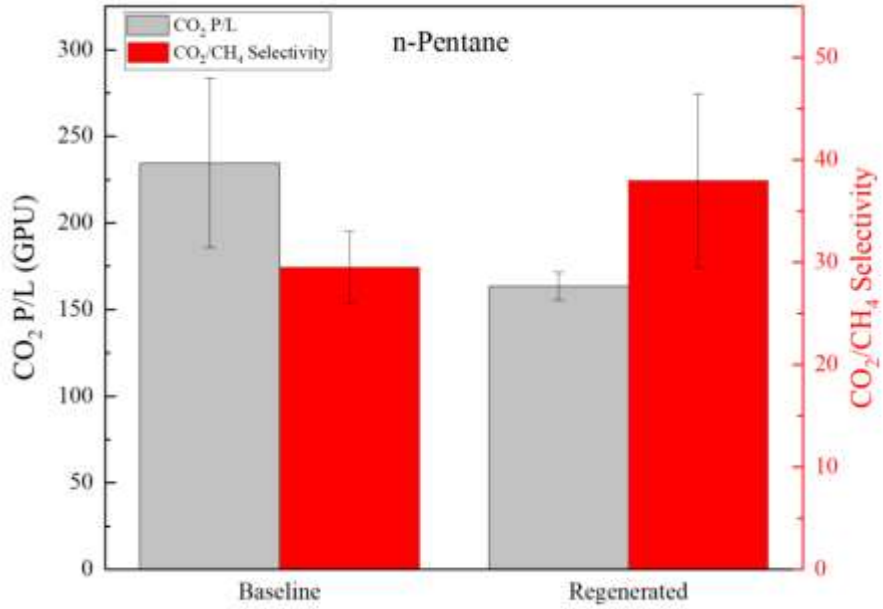
CO2 P/L
CO2/CH4 Selectivity
n-Pentane
CO2 P/L (GPU)
CO2/CH4 Selectivity
300
250
200
150
100
50
0
50
40
30
20
10
0
Baseline
Regenerated

b)

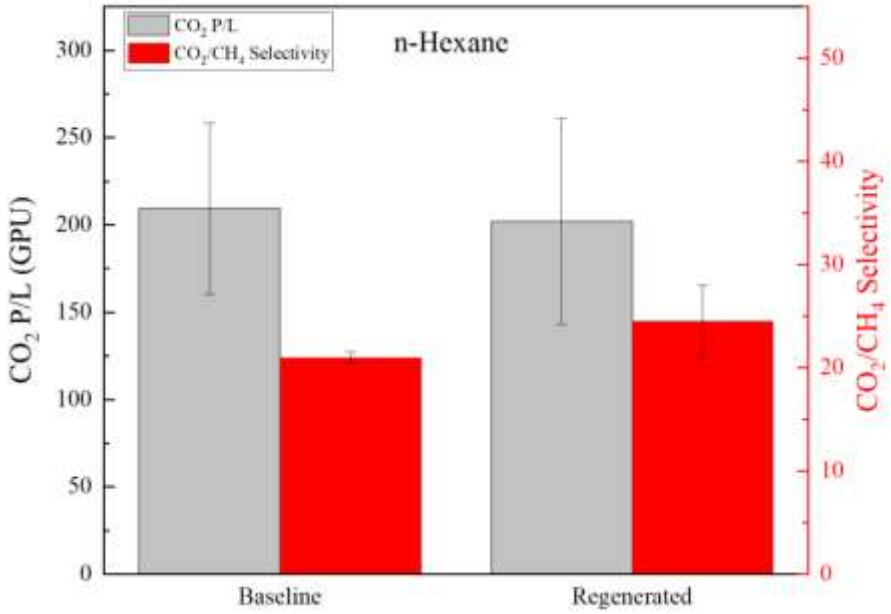
CO2 P/L
CO2/CH4 Selectivity
n-Hexane
CO2 P/L (GPU)
CO2/CH4 Selectivity
300
250
200
150
100
50
0
50
40
30
20
10
0
Baseline
Regenerated

c)

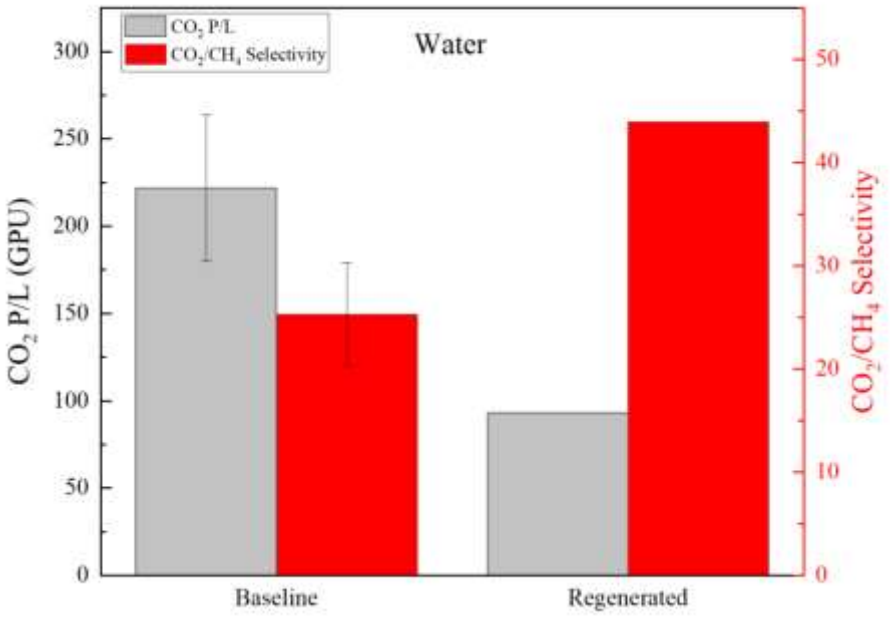

Figure 4.3. CO_2 permeance and CO_2/CH_4 selectivity for baseline and regenerated 6F-derived 550 °C UHP Ar CMS hollow fiber membranes. C_3H_6 regeneration performed for 72 hours after exposure to a) n-pentane, b) n-hexane, or c) water for 24 hours. All permeation tests performed at 35 °C using an upstream pressure of 100 psia 50:50 CO_2/CH_4 and downstream pressure of 0 psia.

Figure 4.3 demonstrates that only n-hexane was properly removed, while modules exposed to n-pentane or water both showed significant drops in permeability, (30% and 58% respectively), and increases in CO_2/CH_4 selectivity (29% and 74% respectively). Due to the short time frame in which this experiment was performed, (5 days), it is very unlikely that these performance changes are due to physical aging. The permeance drop in modules exposed to water possibly can be attributed to a clustering effect well established in the field of polymer membranes. As mentioned, saturation of the micropore was hypothesized to be necessary for physical aging prevention, requiring high relative humidity levels for

CMS saturation with water. However, at such high activity levels, molecules capable of hydrogen bonding, such as water, have been shown to cluster, requiring breaking of the cluster or providing a diffusion pathway large enough for the cluster to move through the membrane[12, 13]. The likelihood of such pore sizes occurring in 6F-derived CMS membranes appears to be very small, due to their demonstrated highly selective, rigid-sieving tendencies mentioned previously. However, this topic of clustering of water molecules in CMS membranes was not pursued further due to the difficulty of removing high activity water.

The difficulty of removing pentane is very interesting, especially considering the ease of removing slightly larger hexane. Table 4.1 highlights the similarities in molecular dimensions between pentane and hexane, with only approximately an angstrom difference in length separating the two. Like with water, this topic was not pursued thoroughly due to the difficulty of removing pentane. However, initial steps were taken to begin to explain this rather interesting phenomenon. These steps are shown in Appendix A.

4.2.3 Physical Aging Studies of Carbon Molecular Sieve Membranes in a Hexane Environment

As hexane was the only storage medium of the initial three selected capable of being removed via C_3H_6 regeneration, aging experiments were only performed using a hexane environment and a nitrogen environment, (serving as a control).

To determine the effectiveness of hexane for minimizing physical aging effects, single CMS fiber modules were prepared, and a baseline was established under the same testing conditions used in Section 4.2.2. Next, the modules were stored for three weeks

under their respective environments: either 50 psia N_2 bubbled through liquid hexane or simply 50 psia N_2. Following the storage period, the modules stored in the hexane environment were treated using the C_3H_6 regeneration procedure described in Section 4.2.2. Both sets of modules were then retested, and the results are shown in Figure 4.4 a-b.

Modules stored in the hexane environment saw a 23% drop in CO_2 permeability and a 33% increase in CO_2/CH_4 selectivity, while modules stored in the nitrogen environment observed a 20% drop in CO_2 permeability and a 23% increase in CO_2/CH_4 selectivity over the three weeks. Rather surprisingly, saturating the CMS micropores with hexane did not appear to affect the rate of physical aging relative to an incredibly simple 50 psia N_2 storage. It is possible that pentane or water may have been more effective at minimizing physical aging effects had it been able to be removed, however improving the regeneration technique was not attempted here. Further explanation of these results is discussed in Section 4.5.2

a)

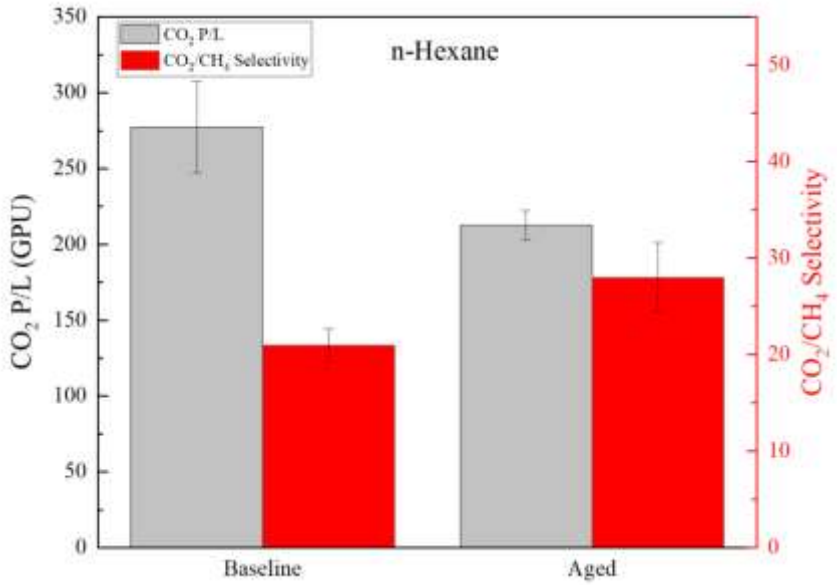

b)

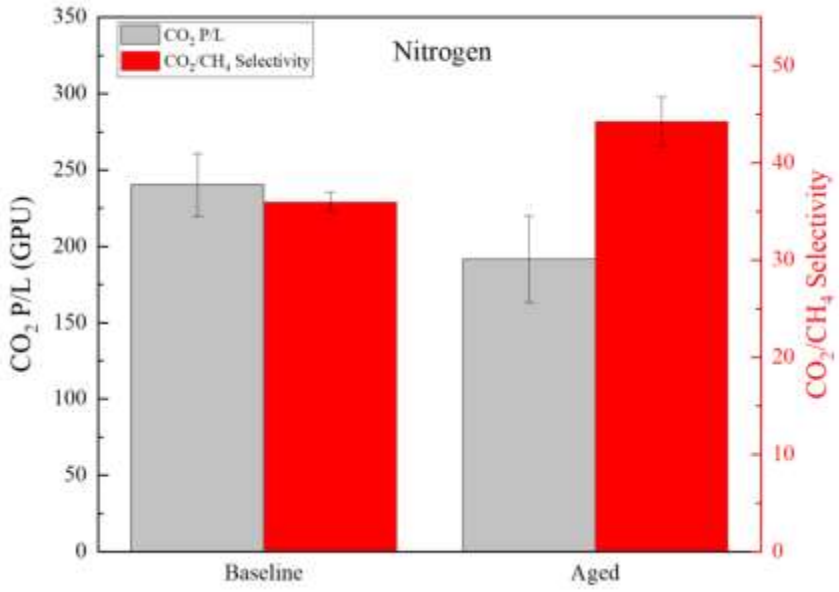

Figure 4.4. CO_2 permeance and CO_2/CH_4 selectivity for baseline and aged 6F-derived 550 °C UHP Ar CMS hollow fiber membranes. Modules were stored for three weeks under a) 50 psia N_2 bubbled through n-hexane, or b) 50 psia N_2. All permeation tests performed at 35 °C using an upstream pressure of 100 psia 50:50 CO_2/CH_4 and downstream pressure of 0 psia.

Additionally, in an attempt to understand the effect of C_3H_6 regeneration, this technique was also used on CMS membranes that had aged under N_2. Surprisingly, the modules showed partially restored CO_2 permeance after C_3H_6 regeneration, suggesting that this technique does more than simply remove organic contaminants. This effect will be discussed further in Section 4.6

4.3 Probing Permeability Changes during Physical Aging in Carbon Molecular Sieve Membranes into Sorption and Diffusion Contributions

Section 4.2.3 raised questions regarding the accuracy of the physical aging mechanism. It seemed rather logical that saturating CMS micropores with large organic molecules would be an effective tool to prop open the CMS structure. Obviously, there are several reasons why such an approach would not work, such as molecular prop flexibility[14], or possibly a situation where the interaction between hexane and the CMS is not strong enough to overcome the thermodynamic tendency for CMS to age. Nevertheless, the results expressed in Section 4.2.3 were interesting enough to warrant a second look at the physical aging mechanism.

To do this, a similar approach to work done by Bernardo et al. was used, where permeability changes due to physical aging were correlated with their respective sorption and diffusion contributions[15]. As mentioned in Chapter 2, the micropores provide relatively large volumes for penetrants to sorb, whereas ultramicropores control the sieving properties of the membrane. Knowing how sorption and diffusion change over the same aging conditions provides guidance for the structural features changing.

4.3.1 Permeance Changes during Physical Aging in Carbon Molecular Sieve Membranes

Figure 4.4-b shows measurable permeance and selectivity changes. For this work, those results were used as the fresh and aged permeability changes. Aging under N_2 is a rather controlled way of aging the membrane, as the environment is inert, but still pressurized slightly, minimizing effects of humidity and other contaminants that may affect the CMS differently.

4.3.2 Sorption Changes during Physical Aging in Carbon Molecular Sieve Membranes

Matching the aging conditions used in Figure 4.4-b, after establishing a baseline sorption isotherm, the sorption sample was stored in 50 psia N_2 for three weeks and then retested. Rather surprisingly, the sample, for both CO_2 and CH_4 isotherms, shows minimal to no sorption changes after three weeks of N_2 storage, highlighted in Figure 4.5. This is in stark contrast with Figure 4.4-b, which showed significant permeance changes. This is also in contrast with the results shown by Xu et al., who documented observable changes to sorption isotherms after lengthy vacuum exposure, albeit on different CMS membranes with different sorbates[3]. Regardless, what Figure 4.5 suggests is that the intrinsic volume of the sample has remained roughly the same after the aging period.

a)

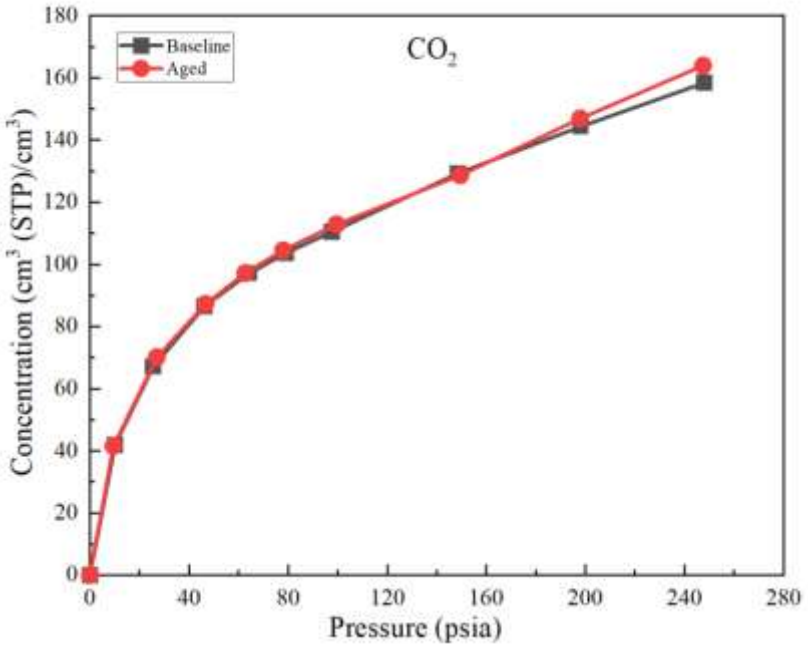

b)

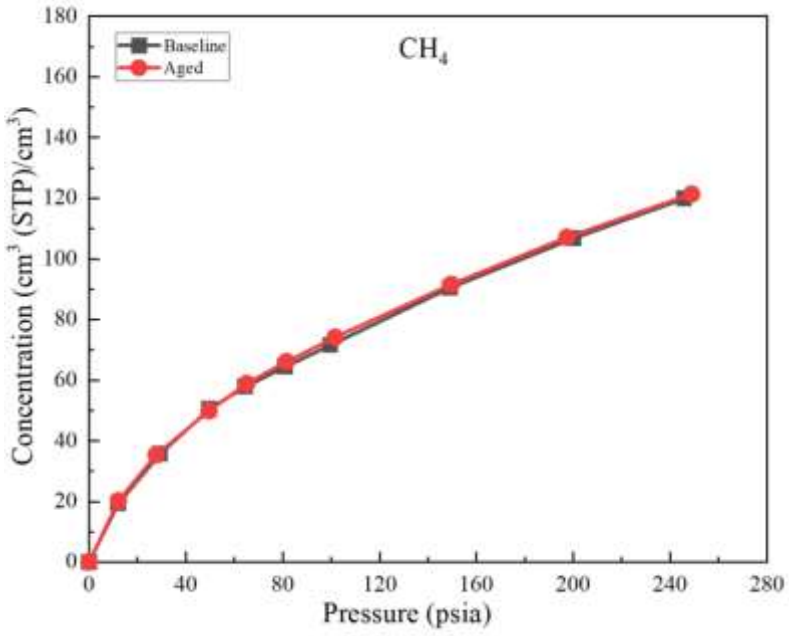

Figure 4.5 Baseline and aged sorption isotherms measured on 6F-derived 550 °C UHP Ar CMS hollow fiber membranes with a) CO_2 and b) CH_4. All isotherms were measured at 35 °C on the same sample[16].

Revisiting the structure of a CMS hollow fiber membrane, it is possible that the porous substructure is affecting the interpretation of Figure 4.5. This region of a CMS hollow fiber still has a sorption capacity, and if that sorption capacity is significantly higher than that in the membrane skin, then any sorption loss in the skin would be effectively "covered up" due to the constant porous substructure. To confirm that the skin intrinsic volume is indeed remaining unchanged, 6F-derived CMS dense films were prepared and the sorption isotherms were measured before and after aging. Currently, it is not certain that the aging rate is thickness dependent as it is in glassy polymer membranes[4, 5, 6, 7]. There is some evidence to suggest this though, shown by Ma et al. on 6FDA-derived CMS and Ogieglo et al. and Ma & Pinnau on PIM-derived CMS[17, 18, 19]. However, to ensure that skin thickness is not a factor at play, much harsher aging conditions were used on the thicker, (~80 microns), dense film than the thinner, (~14 micron), skin of the hollow fiber. After establishing the baseline sorption isotherm for CO_2 on the dense film sample, the film was stored under vacuum for 30 days and then retested. The isotherms are shown in Figure 4.6.

Consistent with Figure 4.5, Figure 4.6 demonstrates essentially the same isotherm before and after the aging period. With essentially no change in sorption capacity being observed in hollow fiber or dense film CMS samples, it is a reasonable approximation to assume then that the relationship between partial pressure, (or fugacity), and equilibrium concentration is approximately constant over the time periods examined.

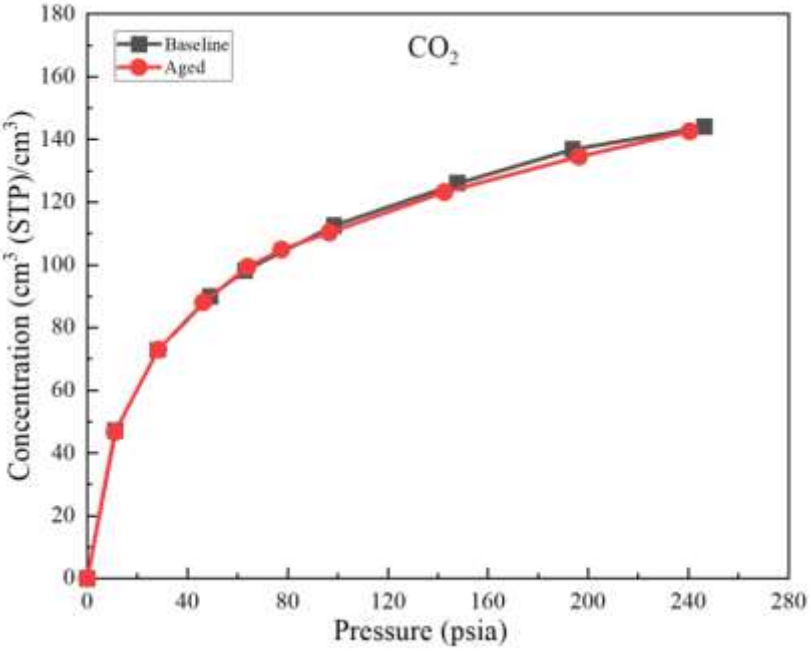

Figure 4.6. Baseline and aged sorption isotherms measured on 6F-derived 550 °C UHP Ar CMS dense film membranes for CO_2. Both isotherms were measured at 35 °C on the same sample. The sole sample was aged for 30 days under vacuum[16].

4.3.3 Diffusion Changes during Physical Aging in Carbon Molecular Sieve Membranes

Combining the results from Sections 4.3.1 and 4.3.2 allow for attributing the permeance changes strictly to changes in the average diffusion coefficient, as represented in Equation 4.1, and demonstrated in Table 4.2

$$\frac{(\mathbb{P}_A/l)_f}{(\mathbb{P}_A/l)_i} = \frac{\mathbb{P}_{A,f}}{\mathbb{P}_{A,i}} = \frac{\mathbb{S}_{A,f}D_{A,f}}{\mathbb{S}_{A,i}D_{A,i}} \approx \frac{D_{A,f}}{D_{A,i}} \tag{4.1}$$

Here subscripts i and f represent the initial and final values of the respective transport coefficient. It is important to note that $\mathbb{P}_A$, $\mathbb{S}_A$, and D_A are all averaged coefficients across

the membrane skin. What Table 4.2 demonstrates is that physical aging in these 6F-derived CMS membranes primarily affects diffusion rather than sorption. Intuitively, this suggests that ultramicropores within CMS plates are tightening, making it less favorable for penetrants to go into the activated state required for a diffusive jump.

Table 4.3 provides additional insight, as it demonstrates that the larger penetrant, CH_4 in this case, is more affected by the physical aging process than the smaller penetrant, CO_2, causing the diffusion selectivity, and thus the permselectivity, to increase.

Table 2. Deconvolution of CO_2 and CH_4 permeation coefficients into diffusion and sorption coefficients on 6F-derived 550 °C UHP Ar CMS hollow fiber and dense film membranes. All modules aged for 3 weeks under 50 psia N_2. All permeation tests performed at 35 °C with an upstream pressure of 100 psia 50:50 CO_2/CH_4 and a downstream pressure of 0 psia.

	Penetrant	Permeance ($\mathbb{P}/l$)	Sorption Coefficient ($\mathbb{S}$)	Thickness Normalized Diffusion Coefficient (D/l)
		$GPU = \frac{10^{-6} cm^3(STP)}{cm^2\ s\ cmHg}$	$\frac{cm^3(STP)}{cm^3\ cmHg}$	$10^{-4}\frac{cm}{s}$
Baseline	CO_2	240.4 ± 20.5	0.36	6.7 ± 0.6
	CH_4	6.7 ± 0.7	0.26	0.3 ± 0.0
Aged	CO_2	191.7 ± 28.4	0.36	5.3 ± 0.8
	CH_4	4.4 ± 0.9	0.26	0.2 ± 0.0

Table 3. Deconvolution of CO_2/CH_4 permselectivity into sorption and diffusion selectivity. All modules aged for 3 weeks under 50 psia N_2. All permeation tests performed at 35 °C with an upstream pressure of 100 psia 50:50 CO_2/CH_4 and a downstream pressure of 0 psia.

	Permselectivity	Sorption Selectivity	Diffusion Selectivity
Baseline	36 ± 1.0	1.4	25.7 ± 0.7
Aged	44.3 ± 2.5	1.4	31.7 ± 1.8

4.4 Envisioned Role of Slit Bypass Pores in Physical Aging of Carbon Molecular Sieve Membranes

In addition to the work deconvoluting permeability coefficients shown above, several auxiliary characterization techniques were done in attempt to provide further insight. Specifically, x-ray diffraction, Raman spectroscopy, and CO_2 physisorption techniques were performed on fresh samples as well as samples aged for one week under vacuum. More specific information regarding the results of these experiments is shown in Appendix B. As expected, these techniques showed minimal to no change in the CMS after vacuum exposure, supporting the conclusions reached in Section 4.3.3 that the physical aging process is much more subtle; most likely consisting of slight tightening of larger ultramicropores. Here we term these larger ultramicropores *slit bypass pores* and believe these are the source of physical aging in CMS membranes. Section 4.4.1 and 4.4.2 will discuss a revised CMS formation process incorporating *slit bypass pores* as well as a more detailed description of how *slit bypass pores* lead to the observed aging results.

4.4.1 Proposed mechanism of formation for slit bypass pores

Section 2.2 discussed the formation pathway from entangled polymer chains in the precursor to the rather organized, microporous CMS structure, first proposed by Rungta and Wenz et al[20]. Briefly stated, it is believed that fragmented polymer chains aromatize into rather linear carbon strands. These strands organize into plates due to the entropic benefit of existing roughly in the same three-dimensional plane, allowing for more translational freedom. The distance between such strands are the feature referred to as ultramicropores, while voids between plates are termed micropores.

During that formation process, imperfect alignment of aromatic strands is probable, given the bimodal pore distribution shown in Figure 2.4. Although the term *slit bypass pore* broadly refers to larger ultramicropores, it is likely that *slit bypass pores* are concentrated at the border of multiple plates. The plate formation process, (alignment of aromatic strands driven by entropic benefits), only truly applies for formation of plates in the same plane. This process is occurring throughout the membrane, forming plates with many different orientations. Given that CMS membranes have exceptional diffusion selectivity, these plates must eventually pack closely enough to sieve molecules with less than an angstrom difference in kinetic diameter. However, this packing of plates is envisioned to be more difficult and imperfect than the arrangement of individual strands into plates, given enough free volume to move such strands. This imperfect packing is believed to be the source of *slit bypass pores* and the formation pathway is summarized in Figure 4.7.

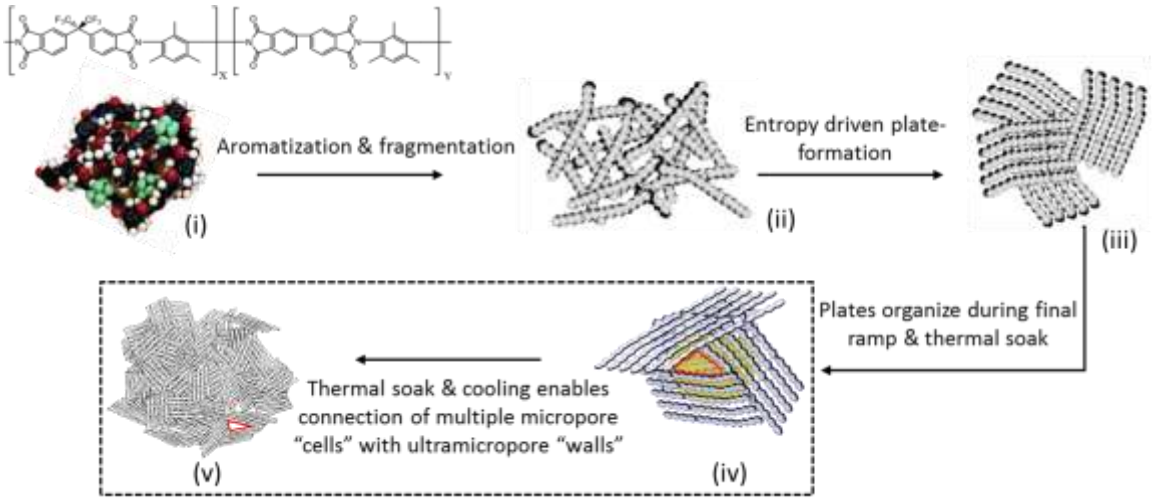

Figure 4.7. Revised 6F-derived CMS formation pathway, highlighting *slit bypass pores* in steps (iv) and (v)[16].

Additionally, a figure relating the hypothetical size of a *slit bypass pore* to the bimodal pore distribution is shown in Figure 4.8. As mentioned above, *slit bypass pores* should be on the larger end of the ultramicropore range, as Table 4.3 illustrates that physical aging affects CH_4 more than CO_2, leading to the increase in diffusion selectivity.

The exact size and distribution of *slit bypass pores* in a CMS membrane should depend heavily on the processing conditions under which the membrane is formed. In a study by Adams et al., it was discovered that moieties are not released from the precursor during pyrolysis until around 500 °C[8]. Accompanying the release of such groups as hydrofluoric acid and fluoroform is the aromatization step and initial arrangement of

aromatic strands into plates. If the pyrolysis process were ended here, *slit bypass pores* should be of high concentration in the membrane, as the membrane has not had significant time to perfect its structure. Further high temperature treatment for longer periods of time should coincide with a more ordered CMS structure, eliminating *slit bypass pores* and making the membrane overall more selective. The pyrolysis protocol used in this work, (standard 550 °C protocol with a two-hour soak), is believed to produce a relatively open CMS structure when compared to CMS membranes pyrolyzed using higher temperature protocols.

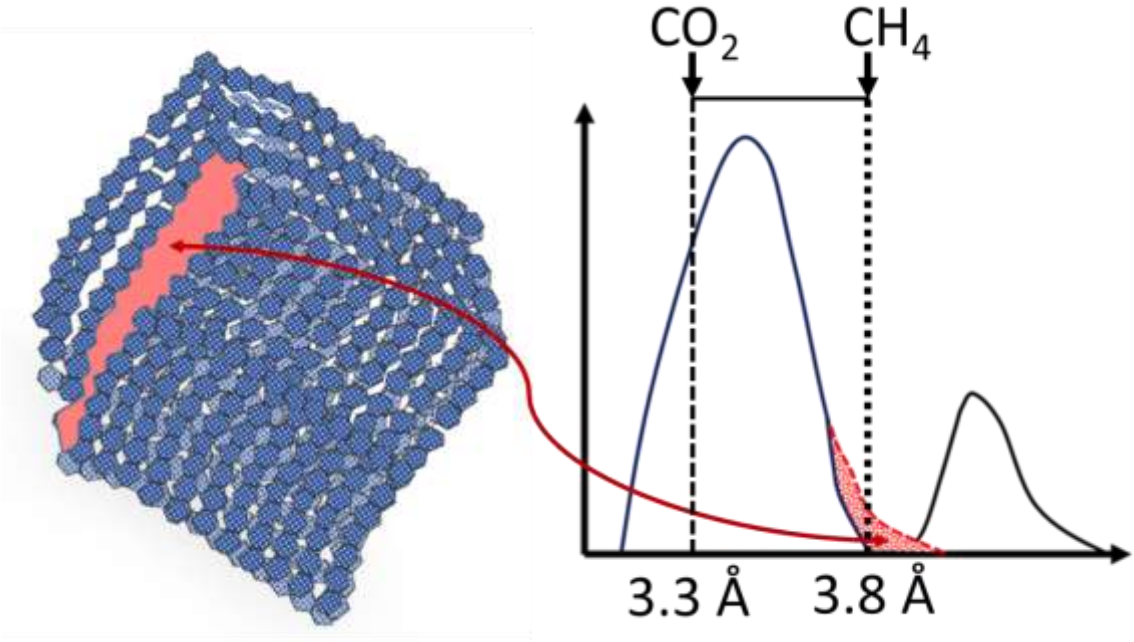

Figure 4.8. Hypothetical *slit bypass pore*, (red), in a micropore cell accompanied with the envisioned CMS bimodal pore distribution with highlighted region representing *slit bypass pore* area[16].

4.4.2 Role of Slit Bypass Pores in Physical Aging of Carbon Molecular Sieve Membranes

Adams et al. proposed the existence of two strand types existing in 6F-derived CMS membranes: one type consisting of pyrrolic groups and one type consisting of pyridinic groups[8]. The structures of these strands are provided in Section 2.3. It is believed that energetic interactions between these strands provide the driving force causing *slit bypass pores* to close, approaching the size of stable ultramicropores[21, 22, 23]. This can be analogized to an argument involving a Lennard-Jones potential.

One can envision a Lennard-Jones diagram existing for only two aromatic strands taken from a CMS membrane. The stable arrangement of these two strands is at some orientation and distance coinciding with an energetic minimum. If the strands are not in such an arrangement, given no kinetic limitations, they will adjust until that energetic minimum is reached. This simple analogy becomes much more complicated when introducing more strands, resembling the case in a CMS membrane, with likely many different local energetic minimums existing within the same Lennard-Jones curve[24]. Regardless, the simple statement that aromatic strands in the CMS move toward *an* energetic minimum should hold true, regardless of where that energetic minimum is on a Lennard-Jones curve. Strands adjacent to a *slit bypass pore* are believed to not be in this envisioned energetic equilibrium, and additionally have the free volume, (given that *slit bypass pores* are larger than typical ultramicropores), to arrange themselves in such a way to approach a stable arrangement. This idea can broadly be represented in Figure 4.9. Such adjustments to *slit bypass pores* can explain the decrease in diffusion coefficients of each penetrant and increase in diffusion selectivity, without greatly affecting the overall sorption capacity, matching the transport trends highlighted in Section 4.3.

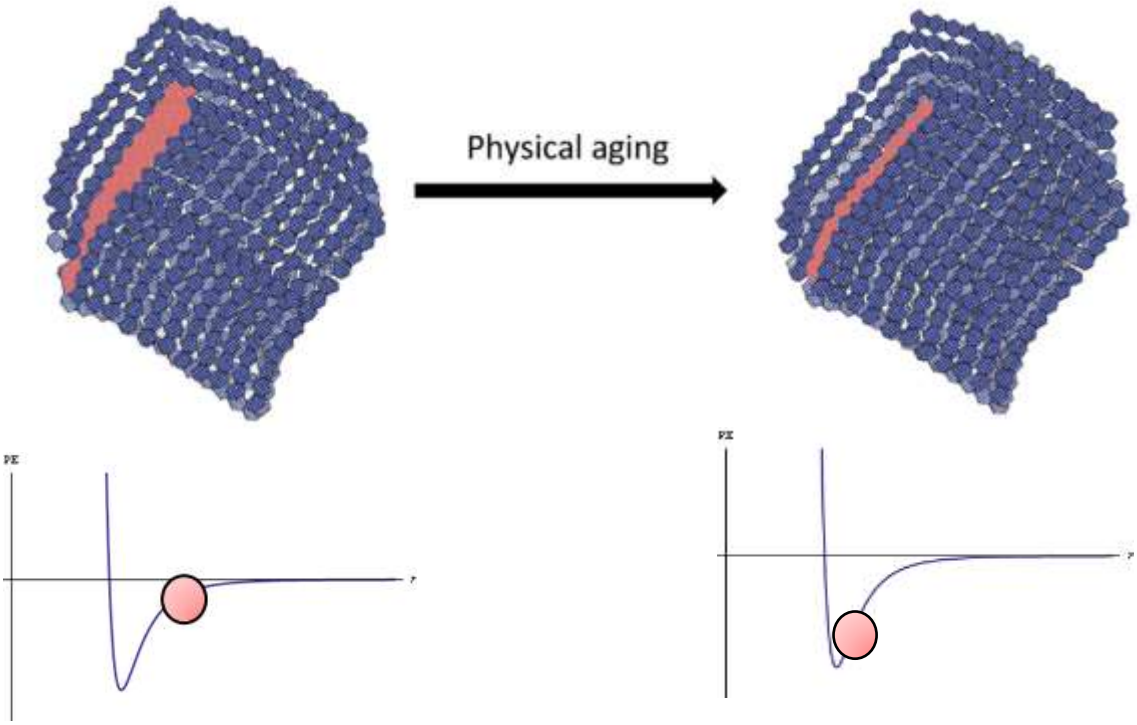

Figure 4.9. Proposed mechanism of physical aging in 6F-derived CMS membranes[16].

4.5 Suppressing Physical Aging in Carbon Molecular Sieve Membranes

With a proposed aging mechanism that fits with experimental observation, this next section will focus on techniques capable of minimizing physical aging effects.

4.5.1 Physical Aging Studies of Carbon Molecular Sieve Membranes under CO_2 Environments

Dr. Graham Wenz first documented the ability of CO_2 to suppress physical aging effects in 6F-derived CMS membranes[25]. The findings were then published by Sanyal et al. in 2018 [26]. Stated briefly, Wenz found that saturating the membrane skin with 115 psia of CO_2 at 25 °C preserved the baseline permeance, with roughly 94% of CO_2 permeance present after 30 days storage and 75% of CO_2 permeance present after 90 days storage [25]. This is significantly better than storage under 50 psia N_2 mentioned previously, which saw 75% of CO_2 permeance left after only 21 days. Applying the revised aging mechanism, it appears that this partial pressure of CO_2 was able to keep open *slit bypass pores,* maintaining performance similar to that of the baseline for a longer period of time.

This important study was recreated for this work using the same testing conditions as those in Figure 4.4 and alike and stored under 115 psia CO_2 for 21 days to match the storage length of previous experiments. Significantly, similar results to Wenz were observed, with approximately 94% of baseline CO_2 permeance remaining after 21 days. This is highlighted in Figure 4.10.

Section 4.3.2 demonstrated that sorption does not change with aging, so it is believed *slit bypass pores* do not provide any significant sorption capacity. Therefore, it is not believed that molecules are sorbing in *slit bypass pores*, propping them open. This would require them to sorb in an activated state, which should be rather unfavorable. It is therefore believed that the CO_2 molecules in the CMS during storage act essentially as a traffic of molecules, with diffusive jumps through *slit bypass pores* perturbing the energetic interactions between adjacent strands. This suggests that the rate of physical aging is a function of the number of diffusive jumps made through *slit bypass pores,* and therefore

indirectly a function of sorbed concentration. If correct, then CMS modules stored under lower concentrations of sorbed CO_2 should age more, and vice versa.

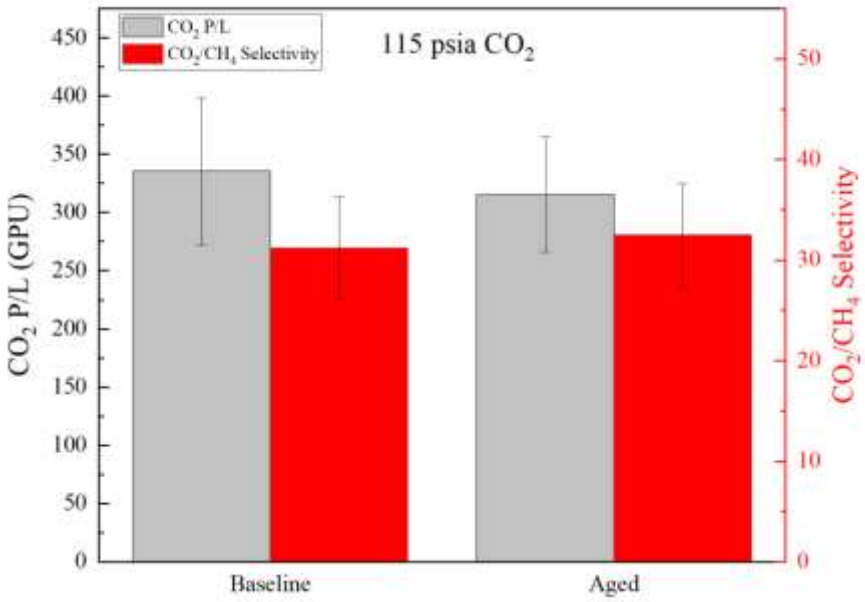

Figure 4.10. CO_2 permeance and CO_2/CH_4 selectivity for baseline and aged 6F-derived 550 °C UHP Ar CMS hollow fiber membranes. Modules were stored for 21 days under 115 psia CO_2 at 25 °C. All permeation tests performed at 35 °C using an upstream pressure of 100 psia 50:50 CO_2/CH_4 and downstream pressure of 0 psia[16].

To gain insight into the sorbed concentration of CO_2 in CMS membranes at a particular partial pressure, a CO_2 sorption isotherm was obtained at 25 °C. Modules are typically stored at 25 °C, so having the CO_2 isotherm at storage temperature provides an indication for the concentration in the module. The CO_2 sorption isotherm at 25 °C is shown in Figure 4.12.

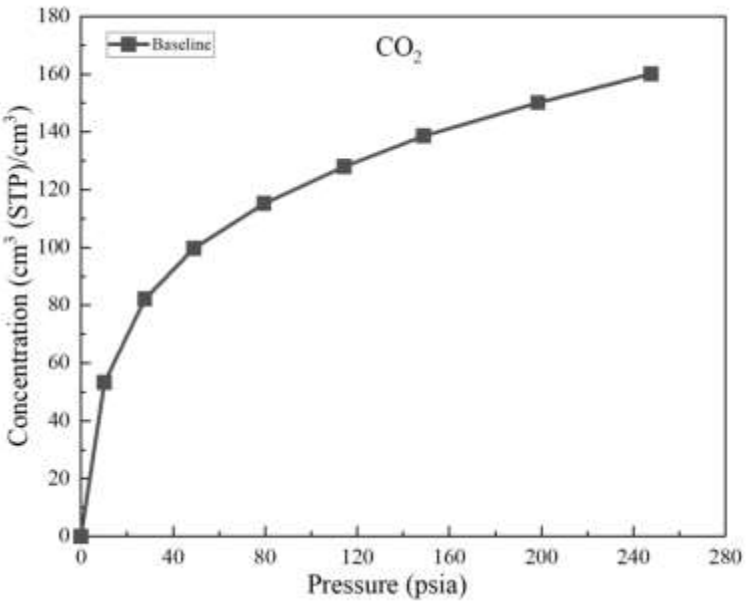

Figure 4.11. Baseline sorption isotherm measured on 6F-derived 550 °C UHP Ar CMS hollow fiber membranes for CO_2. The isotherm was measured at 25 °C[16].

With this input from the sorption isotherm, two additional points were selected to store CMS membranes. 28 psia and 247 psia were selected, as they provide a wide range of sorbed concentration, without needing incorporation of a vacuum. Testing procedures followed the same steps as those for storage under 115 psia, and the results are shown in Figure 4.12.

a)

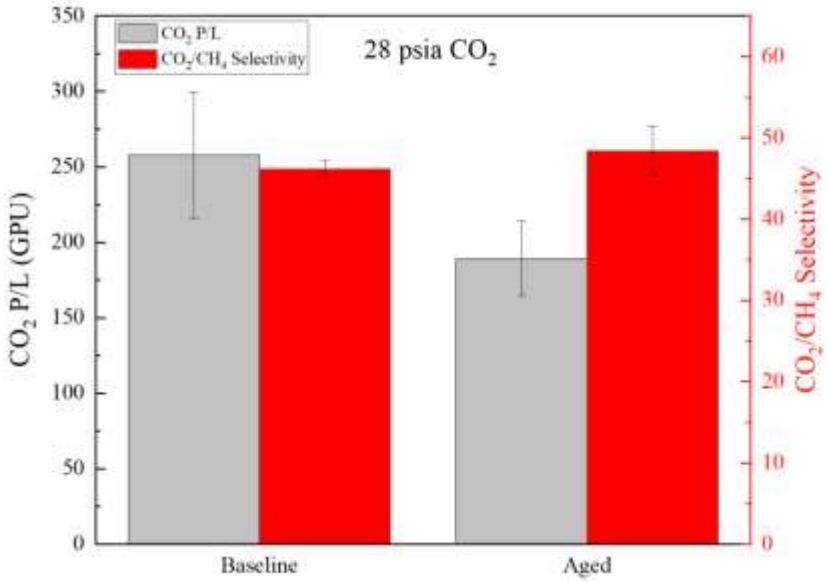

b)

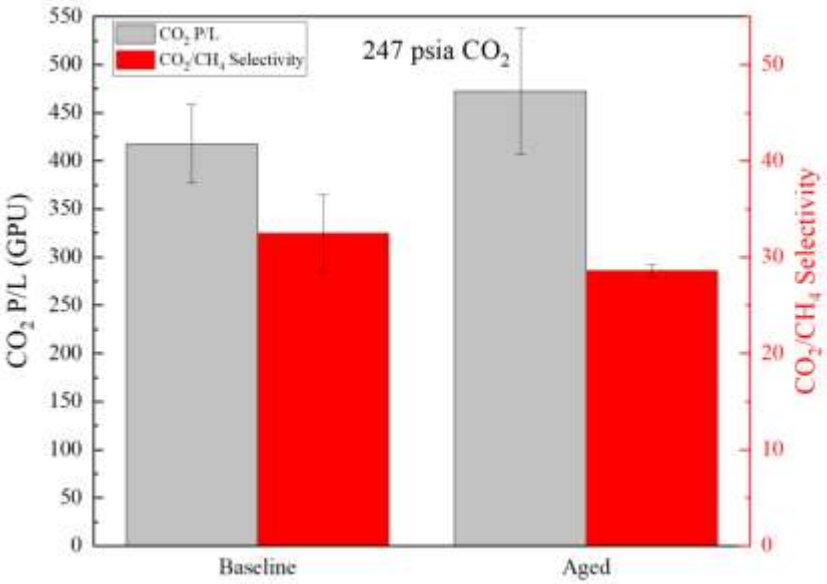

Figure 4.12. CO_2 permeance and CO_2/CH_4 selectivity for baseline and aged 6F-derived 550 °C UHP Ar CMS hollow fiber membranes. Modules were stored for 21 days at 25 °C under a) 28 psia CO_2 and b) 247 psia CO_2. All permeation tests performed at 35 °C using an upstream pressure of 100 psia 50:50 CO_2/CH_4 and downstream pressure of 0 psia.

Interestingly, Figure 4.12 demonstrates rather nicely that the rate of physical aging is related to the sorbed concentration. As mentioned previously, it is believed that the higher concentration of a particular sorbed penetrant, the higher the number of diffusive jumps through *slit bypass pores*. This in turns prevents the *slit bypass pores* from contracting, preserving their initial dimensions. It is important here to distinguish between *jump frequency* and the number of diffusive jumps. Jump frequency is a defined term related to the activation energy and entropy. No statement is made here to discuss how jump frequency might or might not be changing with concentration. The statement above simply implies that the absolute number of jumps increases with increasing concentration, as there are more molecules able to jump.

It is important to note that modules stored under 247 psia CO_2 for three weeks observed a partial CO_2 permeance increase, (13%), as well as a slight decrease in CO_2/CH_4 selectivity, (-12%). Such a change in membrane performance would be consistent with *slit bypass pore* dilation, as suggested by Table 4.3. Section 4.6 will attempt to shed light on this phenomenon and the regeneration effect described in 4.2.3.

4.5.2 Physical Aging of Carbon Molecular Sieve Membranes under C_3H_6

Physical aging studies under CO_2 environments were incredibly insightful, as it strongly suggested that the rate of separation performance change is a function of concentration. However, as suggested by Section 4.2.3, not all environments, (or concentrations), are created equal in terms of aging suppression. Storage under a hexane environment was not as effective as storage under 115 psia CO_2, and roughly similar to storage under 28 psia CO_2. This is even considering that the CMS was entirely saturated with hexane, while it was not so in the two CO_2 storage cases. Rather obviously, there is

a difference in number of moles when comparing these cases, with more molecules sorbed at 28 psia CO_2 than when the CMS is completely saturated with hexane. This suggests that it cannot simply be percent saturation that defines a specific storage technique's ability to suppress aging.

Storage under C_3H_6 can shed further light on possible factors may be contributing to aging suppression. Importantly, at 28 psia and 25 °C, roughly the same number of molecules of either CO_2 or C_3H_6 are sorbed in the CMS, providing an excellent comparison. The sorption isotherm for C_3H_6 at 25 °C is shown in Figure 4.13.

Comparing Figure 4.12 to Figure 4.14, approximately 80 cm^3 (STP)/cm^3 is sorbed in the CMS at 28 psia in both isotherms. Mirroring storage under 28 psia CO_2, baseline permeance and selectivity were established, and modules were stored for three weeks under 28 psia C_3H_6, then retested. The results from this work are shown in Figure 4.14. After three weeks, the modules stored under C_3H_6 retained roughly 91% of their original CO_2 permeance, better than the storage under 28 psia of CO_2, which retained 77% of the original CO_2 permeance.

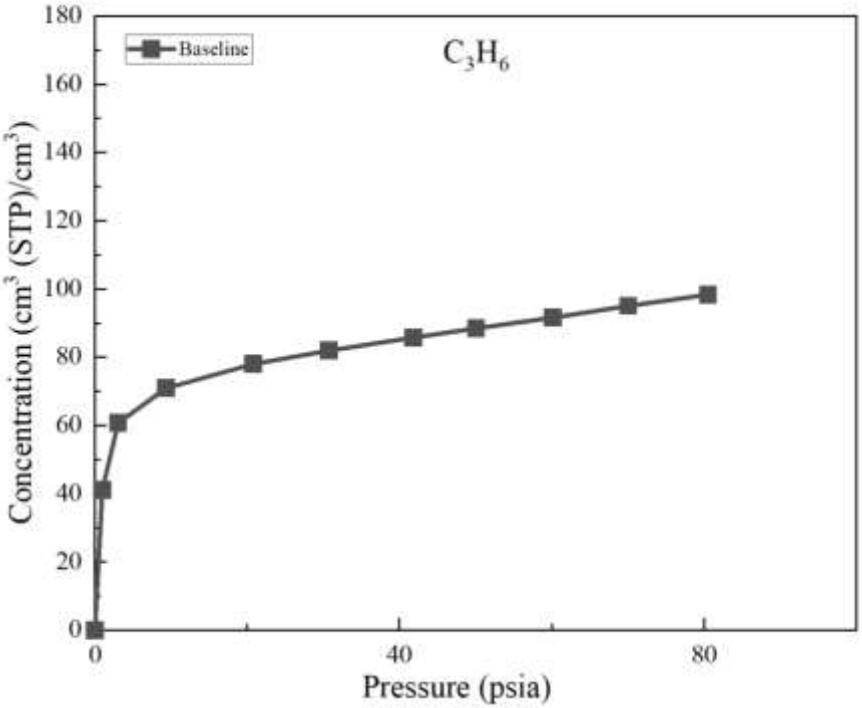

Figure 4.13. Baseline sorption isotherm measured on 6F-derived 550 °C UHP Ar CMS dense film membranes for C_3H_6. The isotherm was measured at 25 °C.

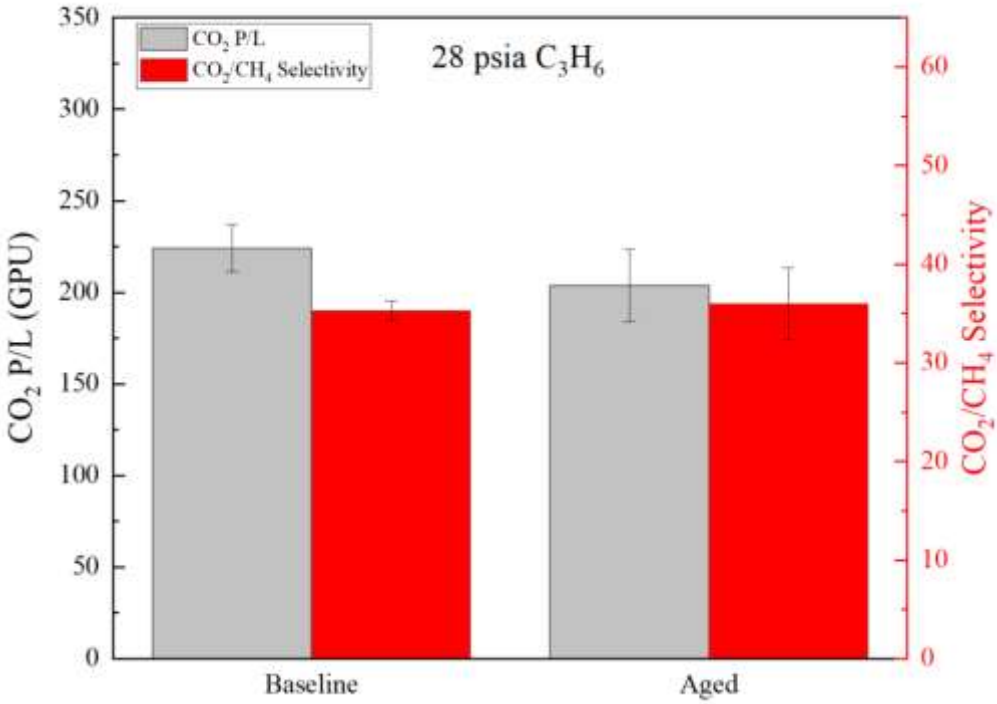

Figure 4.14. CO_2 permeance and CO_2/CH_4 selectivity for baseline and aged 6F-derived 550 °C UHP Ar CMS hollow fiber membranes. Modules were stored for 21 days at 25 °C under 28 psia C_3H_6. All permeation tests performed at 35 °C using an upstream pressure of 100 psia 50:50 CO_2/CH_4 and downstream pressure of 0 psia[16].

Relating this result back to the proposed aging mechanism established in Section 4.4.2, C_3H_6 must have a stronger ability, per molecule, to preserve *slit bypass pores*. As one can expect, the average activated diffusion coefficient for C_3H_6 is lower than that for CO_2. Although not measured for this work, it is reasonable to suspect that the activation energy of diffusion is higher for C_3H_6 than CO_2, leading to a lower jump frequency. What this would suggest is that for a given CMS membrane saturated with either CO_2 or C_3H_6, all other variables equal, there would be fewer diffusive jumps made by C_3H_6. However, Figure 4.14 demonstrated that even with fewer jumps, *slit bypass pores* remained more

open under C_3H_6 than CO_2 with roughly the same number of moles present. Additionally, as Section 4.3.2 noted, the intrinsic volume of the CMS remains relatively unchanged, leading to a constant sorption capacity. Therefore, each diffusive jump made by C_3H_6 should be more effective at perturbing the energetic interactions made by strands across *slit bypass pores*, assuming the molecule has access to *slit bypass pores*.

Collectively, what these results indicate is that there are a number of variables that define a storage medium's ability to suppress physical aging, possibly including sorbed concentration, percent saturation, size, shape, affinity for CMS, and possibly others. Further work is required to more concretely describe these results. However, they are all supported by Section 4.3.2, noting that sorption in 6F-derived CMS membranes has a constant relationship with partial pressure over time, relying solely on diffusion changes to explain drops in permeability. Table 4.4 provides a summary of storage conditions and aging suppression.

Table 4.4. Summary of storage concentration performance minimizing physical aging effects. All storage performed for three weeks at 25 °C.

Storage Medium	Storage Concentration at 25 °C cm^3 (STP)/cm^3	$\frac{\mathbb{P}_{CO_2,f}}{\mathbb{P}_{CO_2,i}}$ -	$\frac{\alpha_{CO_2/CH_4,f}}{\alpha_{CO_2/CH_4,i}}$ -
n-C_6H_{14}	~ 59.3	0.77 ± 0.05	1.33 ± 0.07
C_3H_6	82.0	0.91 ± 0.05	1.02 ± 0.04
CO_2	82.1	0.74 ± 0.02	1.05 ± 0.09
CO_2	128	0.95 ± 0.07	1.04 ± 0.07
CO_2	160.1	1.13 ± 0.12	0.89 ± 0.12

4.6 Reversing Physical Aging in Carbon Molecular Sieve Membranes

Thus far in this chapter, there have been two instances of an apparent permeance improvement in a CMS membrane. The first being noted in Section 4.2.3 when, after three weeks of 50 psia N_2 storage, the aged modules were exposed to the C_3H_6 regeneration treatment first used by Jones[10]. The second being in Section 4.5.1 after storage of modules under 247 psia CO_2 at 25 °C. Such results have been documented in several other publications[10, 27, 28]. However, the exact reason for such behavior is still unknown. This section does not define the process entirely but does take steps to shed light on what might be happening mechanistically within the CMS.

Initially, as mentioned in Section 4.2.3, a control experiment was performed to determine if the C_3H_6 regeneration technique was simply removing the organic

contaminants or if it was having a dilating effect on the CMS. Upon exposing the aged hollow fiber samples to the C_3H_6 treatment, some of the lost permeance was recovered. This is illustrated in Figure 4.15.

Although the increase in permeance is rather small, it is still interesting. What this suggests is that the C_3H_6 treatment might be restoring some of the permeance lost due to physical aging. To ensure that these samples had not been contaminated with unexpected organics, similar experiments were performed, but modules were aged under vacuum rather than N_2. The results of this work are shown in Figure 4.16.

Even after a significant drop, CO_2 permeance was able to be restored to within 15% of the baseline value. It is important to note that in Figure 4.15 and Figure 4.16, the permeance was not fully restored, meaning there is some apparently permanent loss. It is not known at this time why this is the case. A possible explanation and steps to either prove or disprove it is discussed in Section 6.3.1.

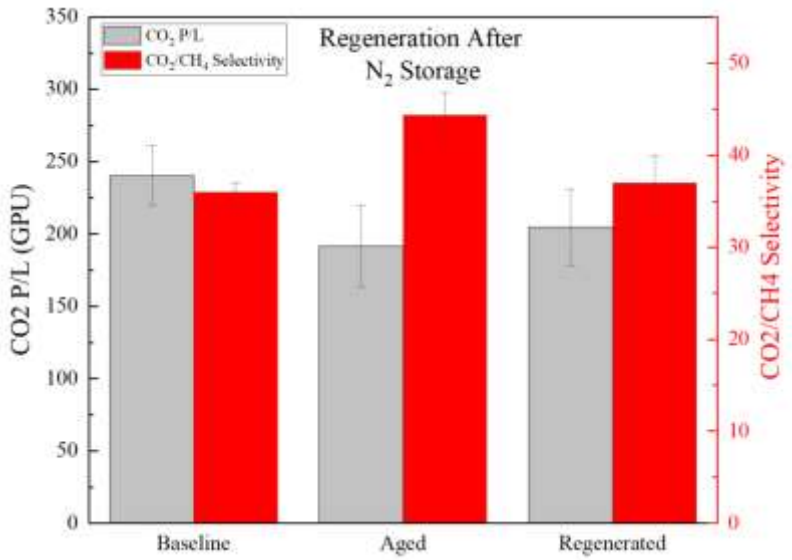

Figure 4.15. CO_2 permeance and CO_2/CH_4 selectivity for baseline, aged, and C_3H_6 regenerated 6F-derived 550 °C UHP Ar CMS hollow fiber membranes. Modules were aged for 21 days at 25 °C under 50 psia N_2. Modules were regenerated for 72 hours at 25 °C under 150 psia C_3H_6. All permeation tests performed at 35 °C using an upstream pressure of 100 psia 50:50 CO_2/CH_4 and downstream pressure of 0 psia.

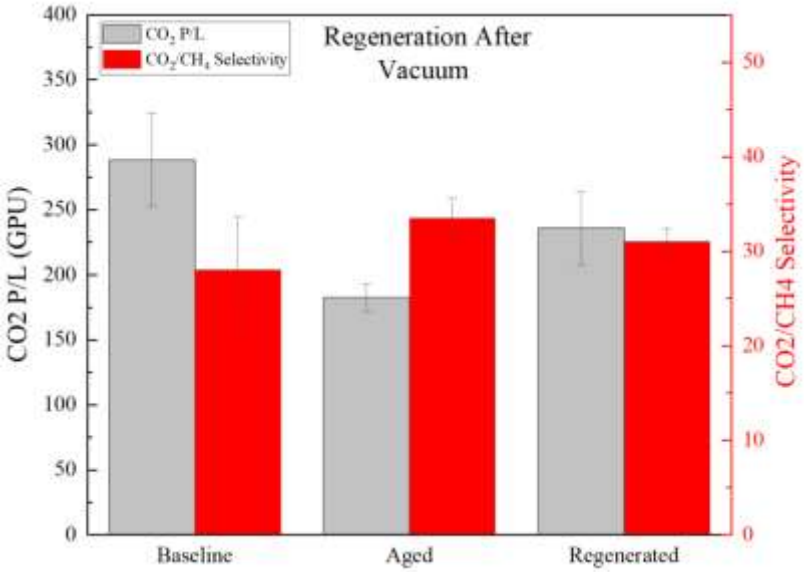

Figure 4.16. CO_2 permeance and CO_2/CH_4 selectivity for baseline, aged, and C_3H_6 regenerated 6F-derived 550 °C UHP Ar CMS hollow fiber membranes. Modules were aged for 18 hours under vacuum at 35 °C. Modules were regenerated for 72 hours at 25 °C under 150 psia C_3H_6. All permeation tests performed at 35 °C using an upstream pressure of 100 psia 50:50 CO_2/CH_4 and downstream pressure of 0 psia.

Similar to steps taken in Section 4.3.2, sorption results before and after the regeneration technique can begin to shed light on the mechanism. As Figure 4.17 demonstrates, the CO_2 isotherm after exposure to high activity C_3H_6 did not change. It is important to note though that the pressure inside the sorption cells was not held at the regeneration pressure for the entirety of the 72 hours. Both the reservoir cell and sample cell were initially pressurized with the necessary amount of C_3H_6, but then the valves were closed, and the C_3H_6 cylinder was removed to be used elsewhere. Because of this, the pressure in the sample cell decreased as the C_3H_6 sorbed in the CMS. It is thought to be unlikely that this change in the protocol altered the conclusions of this experiment. However, this experiment could be repeated while maintaining a constant pressure in the cell to ensure that the conclusion reached here is correct.

Like the conclusions reached in Section 4.3, this suggests that the changes are primarily affecting the diffusion coefficient in CMS membranes. Again, considering the observed mobility of *slit bypass pores*, it suggests then that C_3H_6 regeneration can slightly dilate this region, making it easier for penetrants to make diffusive jumps. Relating to the concept of a "traffic" of molecules mentioned earlier, this result, in addition to the result shown in Figure 4.12, seems to imply that if diffusive jumps are frequent and impactful enough, they can in fact increase permeance.

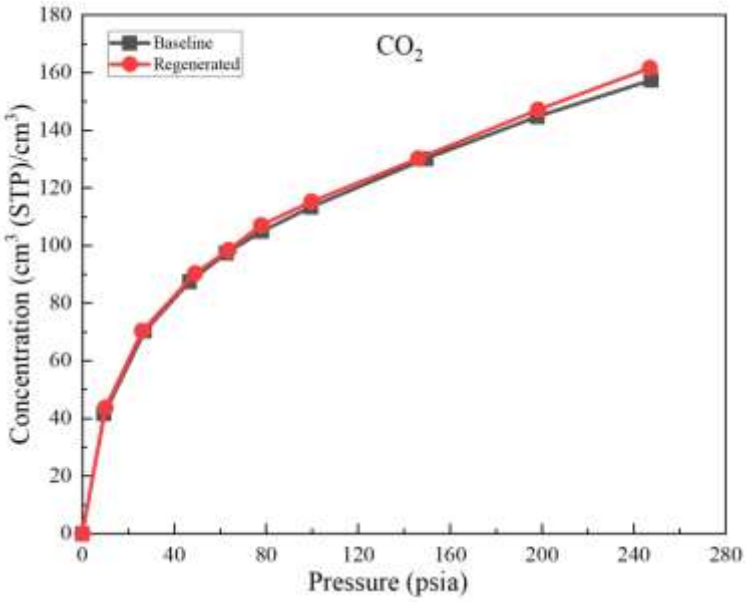

Figure 4.17. Baseline and regenerated sorption isotherms measured on 6F-derived 550 °C UHP Ar CMS hollow fiber membranes for CO_2. Both isotherms were measured at 35 °C on the same sample. The sample was regenerated for 72 hours under high activity C_3H_6.

It has been suggested that pi-electrons may play a key role in this regeneration process[27]. In this explanation, the higher electron density in these pi bonds is envisioned to repel the electron clouds of the aromatic strands. Such an explanation would relate to the results observed here, where high concentrations of CO_2 and C_3H_6 have produced a regeneration effect. To test the validity of this explanation, the regeneration technique was performed on aged CMS hollow fibers, as before, but using high activity C_3H_8 in place of C_3H_6, thus removing the possible effects of pi bonds in the storage medium. As Figure 4.18 demonstrates, some of the CO_2 permeance lost due to aging was able to be recovered. Not enough can be said at this time if C_3H_6 is better at regenerating aged CMS than C_3H_8.

It does demonstrate though that pi-bonds are not necessary for this effect to occur, which is important, nonetheless.

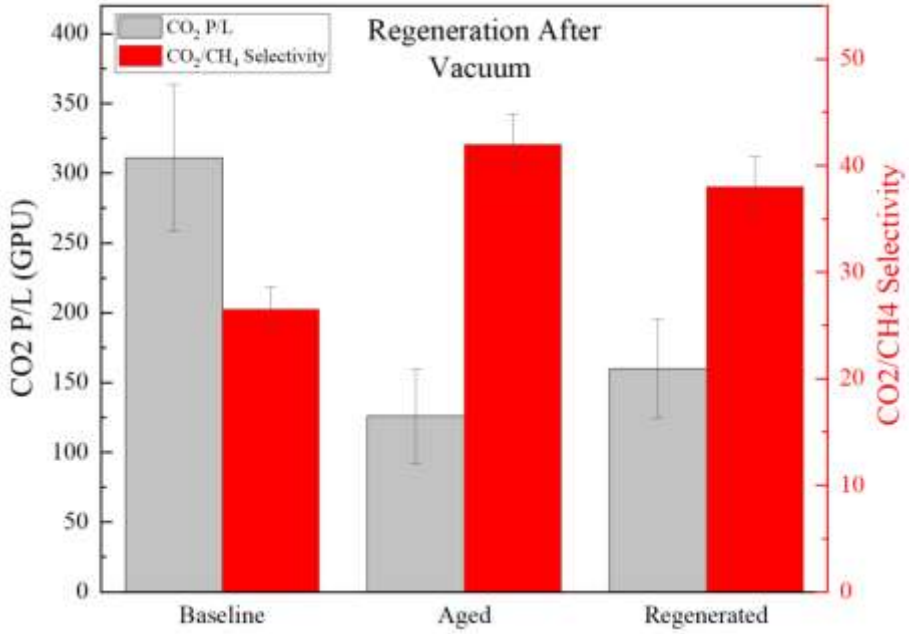

Figure 4.18. CO_2 permeance and CO_2/CH_4 selectivity for baseline, aged, and C_3H_8 regenerated 6F-derived 550 °C UHP Ar CMS hollow fiber membranes. Modules were aged for 18 hours under vacuum at 35 °C. Modules were regenerated for 72 hours at 25 °C under 125 psia C_3H_8. All permeation tests performed at 35 °C using an upstream pressure of 100 psia 50:50 CO_2/CH_4 and downstream pressure of 0 psia.

Although there is much still unknown about this technique, it does present a rather feasible solution to reverse physical aging in CMS membranes. Section 4.6 has demonstrated that C_3H_6 regeneration most likely has an impact on diffusion coefficients, slightly dilating the structure. If such a statement is true, *slit bypass pores* would provide the ideal place for such dilation, as these sites are believed to not quite be at an energetic equilibrium, meaning the attractive interactions between strands are not as strong and thus more easily perturbed.

Regardless of the exact mechanism, consistent with other findings, these results suggest a flexibility in the carbon structure[27, 28, 29, 30]. Although CMS membranes have demonstrated exceptional diffusion selectivity confirming it is a rather rigid sieve, the strands performing the sieving can still be perturbed to either open or close, even after the membrane has cooled from pyrolysis temperature.

4.7 References

1. Baker RW, Low BT. Gas separation membrane materials: a perspective. *Macromolecules* 2014, **47**(20)**:** 6999-7013.

2. Galizia M, Chi WS, Smith ZP, Merkel TC, Baker RW, Freeman BD. 50th anniversary perspective: polymers and mixed matrix membranes for gas and vapor separation: a review and prospective opportunities. *Macromolecules* 2017, **50**(20)**:** 7809-7843.

3. Xu L, Rungta M, Hessler J, Qiu W, Brayden M, Martinez M, *et al.* Physical aging in carbon molecular sieve membranes. *Carbon* 2014, **80:** 155-166.

4. McCaig M, Paul DR. Effect of film thickness on the changes in gas permeability of a glassy polyarylate due to physical agingPart I. Experimental observations. *Polymer* 2000, **41**(2)**:** 629-637.

5. McCaig M, Paul DR, Barlow J. Effect of film thickness on the changes in gas permeability of a glassy polyarylate due to physical agingPart II. Mathematical model. *Polymer* 2000, **41**(2)**:** 639-648.

6. Huang Y, Paul DR. Physical aging of thin glassy polymer films monitored by gas permeability. *Polymer* 2004, **45**(25)**:** 8377-8393.

7. Huang Y, Wang X, Paul DR. Physical aging of thin glassy polymer films: Free volume interpretation. *Journal of Membrane Science* 2006, **277**(1-2)**:** 219-229.

8. Adams JS, Itta AK, Zhang C, Wenz GB, Sanyal O, Koros WJ. New insights into structural evolution in carbon molecular sieve membranes during pyrolysis. *Carbon* 2019, **141:** 238-246.

9. Jiménez-Cruz F, Laredo GC. Molecular size evaluation of linear and branched paraffins from the gasoline pool by DFT quantum chemical calculations. *Fuel* 2004, **83**(16)**:** 2183-2188.

10. Jones CW, Koros WJ. Carbon molecular sieve gas separation membranes-II. Regeneration following organic exposure. *Carbon* 1994, **32**(8)**:** 1427-1432.

11. Jones CW, Koros WJ. Carbon molecular sieve gas separation membranes-I. Preparation and characterization based on polyimide precursors. *Carbon* 1994, **32**(8)**:** 1419-1425.

12. Barrie JA, Platt B. The diffusion and clustering of water vapour in polymers. *Polymer* 1963, **4:** 303-313.

13. Nguyen Q, Favre E, Ping Z, Neel J. Clustering of solvents in membranes and its influence on membrane transport properties. *Journal of membrane science* 1996, **113**(1)**:** 137-150.

14. Zerbi G, Roncone P, Longhi G, Wunder SL. Molecular flexibility of polymethylene molecules: A Raman spectroscopic study. *The Journal of chemical physics* 1988, **89**(1)**:** 166-173.

15. Bernardo P, Bazzarelli F, Tasselli F, Clarizia G, Mason C, Maynard-Atem L, *et al.* Effect of physical aging on the gas transport and sorption in PIM-1 membranes. *Polymer* 2017, **113:** 283-294.

16. Hays SS, Sanyal O, León NE, Arab P, Koros WJ. Envisioned role of slit bypass pores in physical aging of carbon molecular sieve membranes. *Carbon* 2020, **157:** 385-394.

17. Ma X, Lin Y, Wei X, Kniep J. Ultrathin carbon molecular sieve membrane for propylene/propane separation. *AIChE Journal* 2016, **62**(2)**:** 491-499.

18. Ogieglo W, Puspasari T, Ma X, Pinnau I. Sub-100 nm carbon molecular sieve membranes from a polymer of intrinsic microporosity precursor: Physical aging and near-equilibrium gas separation properties. *Journal of Membrane Science* 2020, **597:** 117752.

19. Ma X, Pinnau I. Effect of film thickness and physical aging on "intrinsic" gas permeation properties of microporous ethanoanthracene-based polyimides. *Macromolecules* 2018, **51**(3)**:** 1069-1076.

20. Rungta M, Wenz GB, Zhang C, Xu L, Qiu W, Adams JS, *et al.* Carbon molecular sieve structure development and membrane performance relationships. *Carbon* 2017, **115:** 237-248.

21. Sierański T. The intricacies of the stacking interaction in a pyrrole–pyrrole system. *Structural Chemistry* 2016, **27**(4)**:** 1107-1120.

22. Futami Y, Ozaki Y, Hamada Y, Wojcik MJ, Ozaki Y. Frequencies and absorption intensities of fundamentals and overtones of NH stretching vibrations of pyrrole and pyrrole–pyridine complex studied by near-infrared/infrared spectroscopy and density-functional-theory calculations. *Chemical Physics Letters* 2009, **482**(4-6)**:** 320-324.

23. Lan Z, Frutos LM, Sobolewski AL, Domcke W. Photochemistry of hydrogen-bonded aromatic pairs: Quantum dynamical calculations for the pyrrole–pyridine complex. *Proceedings of the National Academy of Sciences* 2008, **105**(35)**:** 12707-12712.

24. De Lange R, Keizer K, Burggraaf A. Analysis and theory of gas transport in microporous sol-gel derived ceramic membranes. *Journal of membrane science* 1995, **104**(1-2)**:** 81-100.

25. Wenz GB. Tuning carbon molecular sieve membrane performance for challenging gas separations. Georgia Institute of Technology, 2017.

26. Sanyal O, Zhang C, Wenz GB, Fu S, Bhuwania N, Xu L, *et al.* Next generation membranes—using tailored carbon. *Carbon* 2018, **127:** 688-698.

27. Haider S, Lindbråthen A, Lie JA, Hägg M-B. Carbon membranes for oxygen enriched air–Part I: Synthesis, performance and preventive regeneration. *Separation and Purification Technology* 2018, **204:** 290-297.

28. Zhang C, Koros WJ. Methods for regenerating aged carbon molecular sieve membranes. Google Patents; 2019.

29. Koresh JE. On the flexibility of the carbon skeleton. *Journal of the Chemical Society, Faraday Transactions* 1993, **89**(6)**:** 935-937.

30. Finkelstein Y, Saig A, Danon A, Koresh J. Encapsulation of He and Ne in carbon molecular sieves. *Langmuir* 2003, **19**(2)**:** 218-219.

CHAPTER 5

DUAL-MODE TRANSPORT IN CARBON MOLECULAR SIEVE MEMBRANES

5.1 Overview

This chapter attempts to create a self-consistent model of CMS membranes, relating structure and the origin of that structure, to observed transport trends. This model bears resemblance to the dual-mobility model describing transport in glassy polymers, however physical connections of the mathematical terms are *quite different between the two models*. This model of transport in CMS membranes and its distinction from glassy polymer transport is described below.

5.2 Dual-mode Sorption in Carbon Molecular Sieve Membranes

Sorption in CMS membranes has been described previously as following a Langmuir sorption model[1, 2, 3]. A Langmuir sorption model can be simplified to three governing assumptions[4]:

1. Sorption occurs only in vacant sites
2. Only monolayer coverage applies
3. Heat of sorption is constant for all sites

Sites, in a loose sense, are treated as available volume for sorbates to exist in a thermodynamically favorable manner.

Close examination of the isotherms, however, reveals substantial deviation from ideal Langmuir sorption. This is demonstrated in Figure 5.1. Such behavior has been documented before on various carbon molecular sieve materials previously approximated

by a single Langmuir environment[5, 6, 7, 8]. There is no shortage of sorption models to correct for these deviations, accounting possibly for unideal behavior of the sorbate or some level of heterogeneity of the sorbent[4, 9]. With this in mind, the combined Langmuir-Henry model is preferred for several reasons that will be discussed.

a)

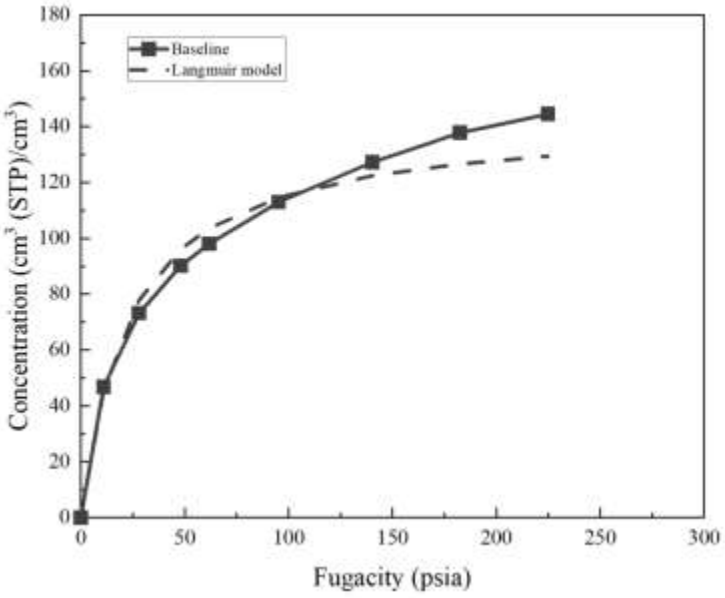

b)

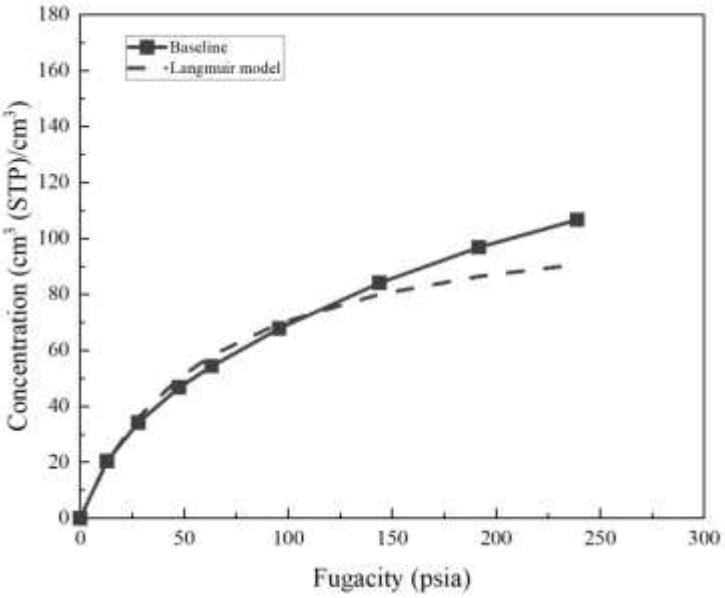

Figure 5.1. Baseline sorption isotherm measured on 6F-derived 550 °C UHP Ar CMS hollow fiber membranes for a) CO_2 and b) CH_4. The isotherms were measured at 35 °C. Dashed line represents the Langmuir sorption model fit to the isotherm. Individual isotherms are averaged from two measured isotherms on the same sample. The error bars on the order of the size of the data points, and equal to the range of measurement. Figures are recreated from Sanyal and Hays et al. (Submitted, Angewandte Chemie).

The Henry's law environment present in CMS is more complex than in a liquid, a rubbery polymer, or even a glassy polymer, but it still has the meaning of a low concentration limit to sorption in an environment in all such cases—including CMS. A dual-Langmuir sorption model might, ideally speaking, provide a greater connection to CMS characteristics. However, as will be shown later, the affinity constant for this second environment appears to be incredibly low, and in the limit of a low affinity constant, a dual-Langmuir model approaches a Langmuir-Henry model. Additionally, assuming a

Langmuir-Henry model allows for relatively easy derivation of flux and permeability equations. Thus, a Langmuir-Henry sorption model allows for a more detailed description of transport in CMS membranes while still maintaining a physical connection to CMS features.

To avoid confusion with the dual-mode sorption model in glassy polymers, terms will be designated with "*C*", standing for *continuous*, in place of "*D*", for *dissolved in glassy polymers*. Additionally, "*L*", meaning *Langmuir*, will be used in place of "*H*", standing for *hole*. These changes can be summarized in Equation 5.1

$$C_i = C_{C,i} + C_{L,i} = k_{C,i} f_i + \frac{C'_{L,i} b_i f_i}{1 + b_i f_i} \tag{5.1}$$

The dual-mode fitting constants for CO_2 and CH_4 sorption isotherms at 35 °C are shown in Table 5.1.

Table 5.1. Dual-mode sorption parameters for CO_2 and CH_4 on 6F-derived 550 °C UHP Ar CMS dense film membranes. Isotherms were measured at 35 °C.

Penetrant	$k_{C,i}$ $\frac{cm^3(STP)}{cm^3\ cmHg}$	b_i $cmHg^{-1}$	$C'_{L,i}$ $\frac{cm^3(STP)}{cm^3}$	K_i -
CO_2	0.037 ± 0.001	0.011 ± 0.000	111.7 ± 0.03	33.9 ± 1.0
CH_4	0.039 ± 0.004	0.005 ± 0.000	68.6 ± 5.1	8.6 ± 1.0

Here, $K_i = \frac{C'_{L,i} b_i}{k_{C,i}}$, is a dimensionless group relating concentrations between the two modes.

5.3 Formation of Two Distinct Environments Within Carbon Molecular Sieve Membranes

To explain the hypothesized formation of the two distinct environments in CMS, once again the CMS formation process must be revisited. One aspect of CMS formation that has not been discussed previously is the likelihood of kinetic hindrances preventing strand accommodation into ultramicroporous plates. It seems reasonable that such hindrances, possibly due to variable strand formation or late aromatization, would restrict mobility in such a way that leaves them "without a home" in an existing plate, and thus termed *orphan strands*. This process can be visualized in Figure 5.2.

As micropores are forming, the rotational freedom of strands is believed to decrease significantly. This should, in turn, make it harder for *orphan strands* to move, leaving them essentially jammed between microporous structures. This vision implies microporous domains surrounded by jammed *orphan strands*, creating two separate environments. The first environment is still within the micropores, providing long diffusion jump lengths and large sorption capacities. Surrounding the micropores is a phase of randomly arranged strands with small volumes trapped between them, creating a more or less continuous diffusive jump pathway for penetrants. This second environment is envisioned to be much less favorable than the environment within micropores, and thus the penetrants are envisioned to be in a more activated state than when they are sorbed in a micropore.

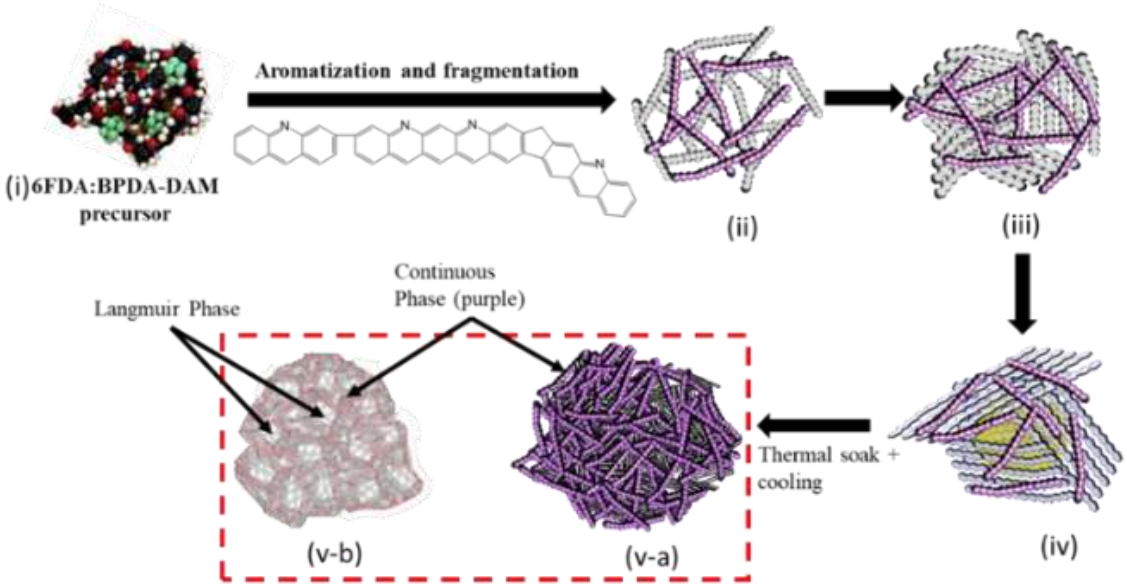

Figure 5.2. Envisioned mechanism for formation of continuous and Langmuir environments in CMS membranes. Microporous domains are envisioned to be surround by the continuous mode (purple strands). This figure is recreated from Sanyal and Hays et al. (Submitted, Angewandte Chemie).

5.4 Mass Transport within Dual-mode Carbon Molecular Sieve Membranes

Transport equations involving dual-mode sorption have been derived several different ways with several different interpretations. The form in this section is used because it also applies to mixed gas feeds, applying to a wide variety of scenarios and is described below.

Total flux can be described as the sum of the fluxes from the two modes, as shown in Equation 5.2.

$$N_i = N_{C,i} + N_{L,i} = -D_{C,i}\frac{\partial C_{C,i}}{\partial x} - D_{L,i}\frac{\partial C_{L,i}}{\partial x} \tag{5.2}$$

From here, equations for permeability can be derived, as shown by Paul & Koros[10]. For a binary mixture, which has been used throughout this report, Koros et al. derived an equation describing mixed gas permeability, shown in Equation 5.3 [11].

$$\mathbb{P}_i = D_{Ci} k_{Ci} \left[1 + \frac{F_i K_i f_{i2}/(f_{i2} - f_{i1})}{1 + b_i f_{i2} + b_j f_{j2}} - \frac{F_i K_i f_{i1}/(f_{i2} - f_{i1})}{1 + b_j f_{i1} + b_j f_{j1}} \right] \tag{5.3}$$

The subscripts "1" and "2" indicate conditions in the downstream and upstream, respectively. F_i is defined as the ratio of $D_{L,i}/D_{C,i}$, providing a dimensionless group indicating the ease which molecules can move through the Langmuir mode vs. the continuous mode.

Current materials characterization techniques lack the ability to provide accurate insight into the CMS structure[12, 13]. Transport has proved the most effective way thus far to shed light on how CMS membranes work. This case is no different. In addition to the peculiar sorption trends noted in Section 5.2, another clue for dual-mode behavior in CMS membranes has been trends in permeability with respect to increasing upstream pressure. Specifically, for a material described by a sole Langmuir environment, such as in some zeolites for example, significant loss in permeability is expected as that material approaches saturation. This behavior has been documented previously[14]. When similar experiments are performed on CMS membranes, essentially pressure-independent permeance is observed. As the upstream pressure is increased, and with a constant downstream pressure of 1 atmosphere, the permeance remained essentially constant. This is illustrated in Figure 5.3. Such behavior has been noted before on CMS formed using the same conditions used here[15]. It is important to note that the variability observed in the

CMS hollow fibers has been noted before and documented in previous publications. Similar trends are observed across all CMS fibers, regardless of their initial permeance.

Figure 5.3 could suggest two possible behaviors occurring in the CMS membrane. First, F_i is very close to zero. Clearly, it cannot actually be zero, as this would violate local equilibrium. Nevertheless, if F_i is very small, then the bracketed term in Equation 5.3 approaches a value of 1 and thus the observed permeability is equal to $D_{Ci}k_{Ci}$. This would give an apparent constant permeability with respect to pressure.

Additionally, $D_{C,i}$ or $D_{L,i}$ might not be constant, and increase with increasing concentration. In such a case, the drop associated with increasing $1 + b_i f_{i2} + b_j f_{j2}$ would be apparently counteracted by increasing of F_i, giving constant permeability.

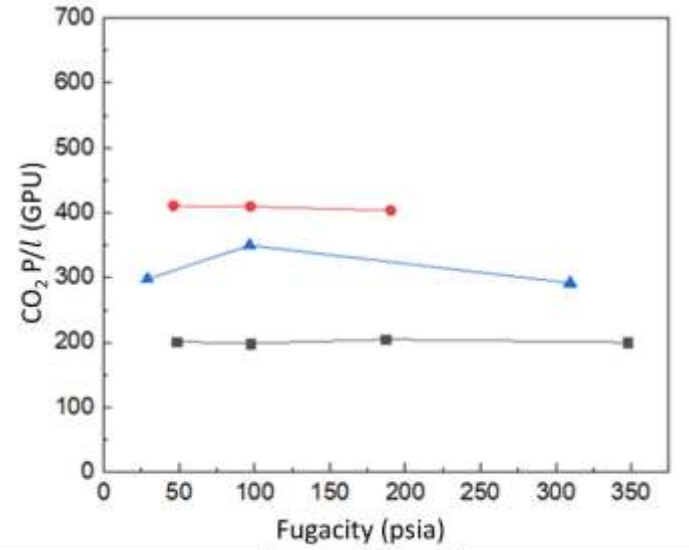

Figure 5.3. Pure CO_2 permeance measured using the constant pressure method. Results from three different single fiber modules are shown. All tests performed at 35 °C. This figure is recreated from Sanyal and Hays et al. (Submitted, Angewandte Chemie)

Mixed gas permeation can shed light on which of these possibilities may have an important effect. By maintaining a constant partial pressure of CO_2, and adjusting the partial pressure of CH_4, F_{CO2} can be calculated by taking the ratio of Equation 5.3 for two conditions. For this work, three different feed conditions were used with a constant CO_2 upstream partial pressure of 50 psia, a constant downstream pressure of 14.5 psia, and a constant temperature of 35 °C:

(i) pure CO_2 at 50 psia

(ii) 50:50 CO_2/CH_4 at 100 psia

(iii) 10:90 CO_2/CH_4 at 500 psia

Table 5.2 and 5.3 display the permeances, selectivities, and calculated F_{CO2}.

Table 5.2. CO_2 permeances and CO_2/CH_4 selectivity obtained on 6F-derived 550 °C UHP Ar CMS hollow fiber membranes. All permeation tests performed at 35 °C with a constant 1 atmosphere downstream. This table is recreated from Sanyal and Hays et al. (Submitted, Angewandte Chemie)

Testing Condition	CO_2 P/*l* (GPU)	$\alpha_{CO2/CH4}$
Pure CO_2 at 50 psia	331.3 ± 13.9	-
50:50 CO_2/CH_4 at 100 psia	268.7 ± 3.3	49.6 ± 1.0
10:90 CO_2/CH_4 at 500 psia	214.7 ± 3.2	23.3 ± 1.7

Table 5.3. F_{CO_2} values from taking a ratio of Equation 5.3 using conditions: (i) pure CO_2 with 50 psia upstream, (ii) 50:50 CO_2/CH_4 with 100 psia upstream, and (iii) 10:90 CO_2/CH_4 with 500 psia upstream. All permeation tests perform at 35 °C with a constant 1 atmosphere downstream. This table is recreated from Sanyal and Hays et al. (Submitted, Angewandte Chemie)

Ratio	F_{CO_2}
(i)/(ii)	0.086 ± 0.015
(i)/(iii)	0.050 ± 0.007
(ii)/(iii)	0.038 ± 0.004

Table 5.3 indicates that F_{CO_2} is very small, but still greater than zero. Additionally, Table 5.2 highlights the ability of CH_4 to compete with CO_2 as the partial pressure of CH_4 is increased. This second point implies that the permeance has not reached an asymptotic value of $D_{C,co_2}k_{C,co_2}/l$, since in that case permeance would have remained relatively constant over the testing conditions used in Table 5.2.

These conclusions suggest that terms, possibly F_i, change with changing concentration. In other words, during pure gas measurements shown in Figure 5.3, F_i might have increased to counteract the decrease associated with increasing $1 + b_i f_{i2}$. However, in the case of a mixed gas, with CH_4 present, and if F_{CO_2} stayed constant, due to the constant CO_2 partial pressure, an increase in the denominator ($1 + b_i f_{i2} + b_j f_{j2}$) would not be counteracted by increasing F_{CO_2}, in the numerator. This situation would lead to the observed CO_2 permeance drop. The dependence of F_i on partial pressure, and other terms for that matter, is not known at this time, and future work is required to shed light on this relationship.

In any case, it is important again to note what such a model means for CMS membranes. Being able to relate a physical picture of the CMS structure containing tunable features to observed transport results creates a self-consistency allowing for controlled steps forward in membrane design. The ability to manipulate the two modes would demonstrate incredible control of transport through CMS membranes, making this work very exciting going forward, presenting many exciting new tuning possibilities.

5.5 References

1. Koresh JE, Soffer A. Mechanism of permeation through molecular-sieve carbon membrane. Part 1.—The effect of adsorption and the dependence on pressure. *Journal of the Chemical Society, Faraday Transactions 1: Physical Chemistry in Condensed Phases* 1986, **82**(7)**:** 2057-2063.

2. Rungta M, Wenz GB, Zhang C, Xu L, Qiu W, Adams JS, *et al.* Carbon molecular sieve structure development and membrane performance relationships. *Carbon* 2017, **115:** 237-248.

3. Ma Y, Zhang F, Deckman HW, Koros WJ, Lively RP. Flux Equations for Osmotically Moderated Sorption–Diffusion Transport in Rigid Microporous Membranes. *Industrial & Engineering Chemistry Research* 2019.

4. Vannice MA, Joyce WH. *Kinetics of catalytic reactions*, vol. 134. Springer, 2005.

5. Barrer R, Robins A. Sorption of mixtures. Part 2.—Equilibria between binary gas mixtures and some zeolites. *Transactions of the Faraday Society* 1953, **49:** 929-939.

6. Barrer R, Robins A. Sorption of mixtures. Part 1.—Molecular sieve separations of permanent and inert gases. *Transactions of the Faraday Society* 1953, **49:** 807-815.

7. Nguyen C, Do D. Dual Langmuir kinetic model for adsorption in carbon molecular sieve materials. *Langmuir* 2000, **16**(4)**:** 1868-1873.

8. Koresh J, Soffer A. Application of the two-site Langmuir isotherm to microporous adsorbents. *Journal of Colloid and Interface Science* 1983, **92**(2)**:** 517-524.

9. Yang RT. *Gas separation by adsorption processes*. Butterworth-Heinemann, 2013.

10. Paul DR, Koros W. Effect of partially immobilizing sorption on permeability and the diffusion time lag. *Journal of Polymer science: Polymer physics edition* 1976, **14**(4)**:** 675-685.

11. Koros WJ, Chern RT, Stannett V, Hopfenberg HB. A model for permeation of mixed gases and vapors in glassy polymers. *Journal of Polymer Science: Polymer Physics Edition* 1981, **19**(10)**:** 1513-1530.

12. Adams JS, Itta AK, Zhang C, Wenz GB, Sanyal O, Koros WJ. New insights into structural evolution in carbon molecular sieve membranes during pyrolysis. *Carbon* 2019, **141:** 238-246.

13. Hays SS, Sanyal O, León NE, Arab P, Koros WJ. Envisioned role of slit bypass pores in physical aging of carbon molecular sieve membranes. *Carbon* 2020, **157:** 385-394.

14. Poshusta JC, Noble RD, Falconer JL. Temperature and pressure effects on CO2 and CH4 permeation through MFI zeolite membranes. *Journal of membrane science* 1999, **160**(1)**:** 115-125.

15. Zhang C, Wenz GB, Williams PJ, Mayne JM, Liu G, Koros WJ. Purification of aggressive supercritical natural gas using carbon molecular sieve hollow fiber membranes. *Industrial & Engineering Chemistry Research* 2017, **56**(37)**:** 10482-10490.

CHAPTER 6

CONCLUSIONS AND RECOMMENDATIONS

6.1 Thesis Overview Summary

With an ever-growing energy demand, the need for more energy-efficient separation methods becomes more apparent. Membranes, over the last several decades, have grown in their status as energy-saving additions, (or alternatives), to existing separation processes. CMS membranes, specifically, combine a unique combination of high processability, high tunability, and strong separation performance over a broad range of separation conditions, making them among the top candidates for implementation into industrial processes.

Even with the many positives of CMS membranes, obstacles remain, such as improving long-term stability. This thesis has attempted to provide a physical mechanism of how the membrane changes with time to guide further studies. Additionally, it has provided several techniques that can sufficiently suppress physical aging under storage conditions.

This thesis also shed light on pressure-dependent transport behavior and related that behavior to a physical interpretation of the CMS structure. Although early, this work has opened doors to several new avenues of future work, further demonstrating the extensive tunability of CMS membranes. Finally, a self-consistent mathematical model, linked to the currently most accepted vision of CMS formation was provided.

6.2. Conclusions

6.2.1 Physical Aging in Carbon Molecular Sieve Membranes

This chapter attempted to fundamentally explain the physical aging phenomenon in 6F-derived CMS membranes. Initially, it was hypothesized that physical aging could be suppressed by storing the membranes under large organics, including n-hexane and n-pentane. These organics would act as temporary pillars to preserve the micropore structure, which could then be removed after the intended storage period. This attempt was unsuccessful however, which raised questions regarding the envisioned mechanism. Breaking down permeability, (or permeance in this case), into its sorption and diffusion contributions before and after aging revealed that over moderate aging scenarios, sorption capacity remained relatively constant. This implies essentially all permeability changes observed are due to changes in the diffusion coefficient.

Here it was proposed that larger ultramicropores, termed *slit bypass pores*, attempt to reach an energetic equilibrium, reducing their dimensions in the process. This slight adjustment in the ultramicropores would not affect the sorption capacity of the membrane but would hinder diffusive jumps through the selective skin, lowering the permeability.

Investigations into the effectiveness of CO_2 storage revealed a concentration dependence to physical aging. Specifically, storage of CMS membranes under higher concentrations correlated with better aging suppression, and vice versa. This suggests that it is the frequent diffusive jumps through the *slit bypass pores* that preserve the performance. However, storage using different species revealed that it is not simply concentration. Storage under C_3H_6, using the same temperature, pressure, and

concentration, was more effective than CO_2. This suggests that one can conclude that in addition to the number of jumps, the interaction the penetrant has with the membrane is also important for aging suppression. A strong storage medium would have a good combination of both characteristics.

Additionally, it was suggested that increasing the concentration enough allows for slight dilation of the ultramicropores, leading to an apparent regeneration effect. It is believed that this observation is related to the regeneration effect noted by Jones & Koros in 1994 [1]. If correct, this technique provides a feasible method of restoring physically aged CMS membranes, extending their longevity.

6.2.2 Dual-mode Transport in Carbon Molecular Sieve Membranes

Chapter 5 introduced a new vision of transport through CMS membranes by introducing the concept of two distinct environments in local equilibrium within the skin. In addition to the large Langmuir mode discussed, it is concluded that adequate evidence exists for a small continuous phase that can be well approximated with Henry's law sorption. Specifically, deviation from Langmuir sorption in addition to seemingly pressure-independent permeance points to a missing feature in prior studies of CMS membranes. The existence of this second mode provides a feasible explanation for these interesting results.

Such a "missing mode" is believed to form due to kinetic limitations of aromatic strands during CMS formation. Possibly due to strand-strand variation or late aromatization, these strands are envisioned to have trouble being accommodated into

existing ultramicroporous plates. This would, in turn, create a small array of unoriented, jammed strands existing between microporous cells.

This vision implies that penetrants permeating through the CMS membrane will continuously be exchanged from microporous regions to continuous regions as they move down the concentration gradient, because local equilibrium must be maintained. It is important to note that this mechanism still allows for molecular sieving, even if diffusive jumps within the continuous mode are less selective. As the penetrants must jump in and out of the Langmuir phase to maintain local equilibrium, they must go into the activated state associated with being in an ultramicropore. Such jumps are the source of the high selectivity characteristic of CMS membranes.

6.3 Recommendations for Future Work

Although new features of CMS membranes have been introduced in this thesis, further work is needed to fully define them. Potential paths forward are discussed below that can shed further light on the hypotheses presented in this work.

6.3.1 Future Work for Physical Aging in Carbon Molecular Sieve Membranes

Seeking a fundamental understanding of the aging phenomenon in CMS membranes has been valuable in revealing several characteristics of the membrane not known previously. The essential lack of change in the sorption capacity over moderate levels of aging was rather surprising, as evidence has been presented previously suggesting the collapse of micropores with time[2]. The results shown by Xu et al. were obtained on CMS pyrolyzed under different conditions using a different precursor, so the broadness of the result shown in Chapter 4 of this work remains in question. Fu et al., additionally,

demonstrated that the amount of sorption loss in CMS varies from precursor to precursor, with some precursors demonstrating minimal to no loss[3]. These other results suggest that the aging mechanism may vary with CMS membranes derived from different precursors and finding out why will undoubtedly shed further light on the inner workings of the CMS structure.

Additionally, it is interesting to consider the implications of this aging mechanism. Petropolous, in 1970, suggested that transport through a membrane is better conceptualized by a chemical potential gradient, rather than a concentration gradient[4]. Here he introduced the idea of local thermodynamic sorption and diffusion coefficients throughout the skin, thus implying local permeability coefficients. Integration of these local permeabilities across the skin, normalized by the skin thickness, leads to the observed permeability. This idea can be demonstrated by Equation 6.1

$$\mathbb{P}_{obs,i} = \frac{\int_0^l \mathbb{P}_i dx}{\int_0^l dx} = \frac{\int_0^l \mathbb{S}_i D_i dx}{\int_0^l dx} \tag{6.1}$$

Section 4.3.2 demonstrated that sorption capacity does not change with time. This can also be interpreted as meaning the relationship between sorbed concentration and fugacity, or chemical potential, is constant in 6F-derived CMS membranes.

It is valuable to reintroduce the concentration gradient in such a discussion, and the general shape of such gradient in the CMS membrane. Crank provided relationships between the concentration-dependent diffusion coefficient and an approximated concentration curve within a membrane skin[5]. For the case in CMS membranes, diffusion coefficients increase with increasing concentration, leading to a general curve shown in

Figure 6.1. It is important to note that this is not the exact shape of the concentration gradient in a CMS membrane skin. It is merely an approximation of the general behavior.

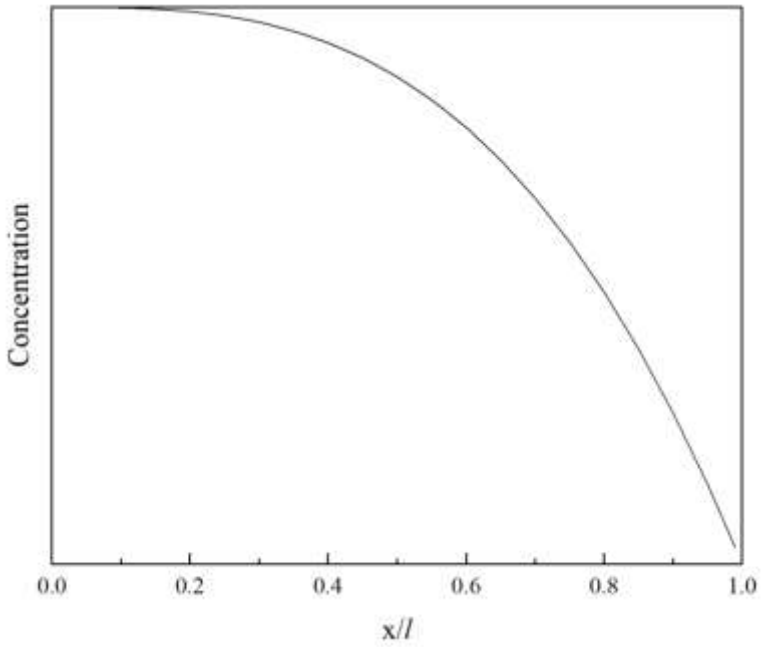

Figure 6.1. Hypothetical concentration gradient present with a CMS membrane skin.

Importantly, Section 4.5.1 of this work demonstrated that the aging rate in CMS is dependent on concentration. It was hypothesized that this is related to the frequency of diffusive jumps through *slit bypass pores* relative to the ability of strand movements. At higher concentrations, a larger number of molecules are in position to make a jump through a *slit bypass pore* in a given unit of time, thereby more strongly perturbing the energetic interactions driving them to close.

Pairing this proposed phenomenon with Petropolous's local permeability coefficients and the specific shape of the concentration gradient in CMS membranes, this suggests the formation of an aging gradient across the membrane skin. If the aging rate in CMS is indeed concentration dependent, then *slit bypass pores* closer to the upstream, (higher concentration), should remain more open than *slit bypass pores* in the downstream, (lower concentration), illustrated by Figure 6.2.

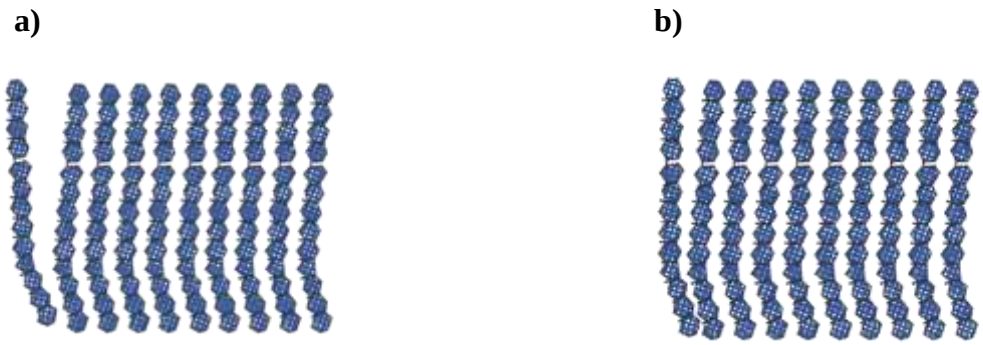

Figure 6.2. Schematic of a CMS plate containing a *slit bypass pore* in the a) upstream and b) downstream during a long-term permeation test. At higher concentrations in the upstream, *slit bypass pores* should be more open. At lower concentration in the downstream, the *slit bypass pores* should be more closed, as jumps through them are less frequent than they would be in the upstream.

This implies that, as the CMS ages, the local permeability coefficients in the downstream should decrease more, proportional to some function of concentration. This concept is illustrated by Figure 6.3. Interestingly, if the area under each respective curve is integrated to estimate the observed permeability, this result leads to behavior resembling

that seen in long-term permeation tests, shown in Figure 6.4. Specifically, it captures the large decrease in permeability initially, with the permeability eventually approaching some stable value.

While this mechanism appears to match trends, more work must be done to determine if there is indeed an aging gradient forming within the CMS. Such an idea can possibly be pursued by permeating gas from shell to bore, then bore to shell. Performing a long-term permeation test with gas permeating from the shell side of the module to the bore side will eventually produce a CMS module with a somewhat stable performance, as illustrated by Figure 6.4b. In such a case, switching the direction of the feed, with gas now permeating from the bore side of the module to the shell side should produce changes to the permeance. Hypothetically, the *slit bypass pores* towards the shell side of the membrane should begin to close, as the concentration in this region is much lower than it was previously. This change should then reveal itself with further decrease in the observed permeance, even though the membrane appeared stable under the previous feed arrangement. If correct, this mechanism should provide a qualitative description of time-dependent transport behavior for many different feed conditions. Knowing the concentration gradient for the specific gas in the CMS membrane, and knowing how effectively that gas prevents aging, should allow for rough predictions of stability.

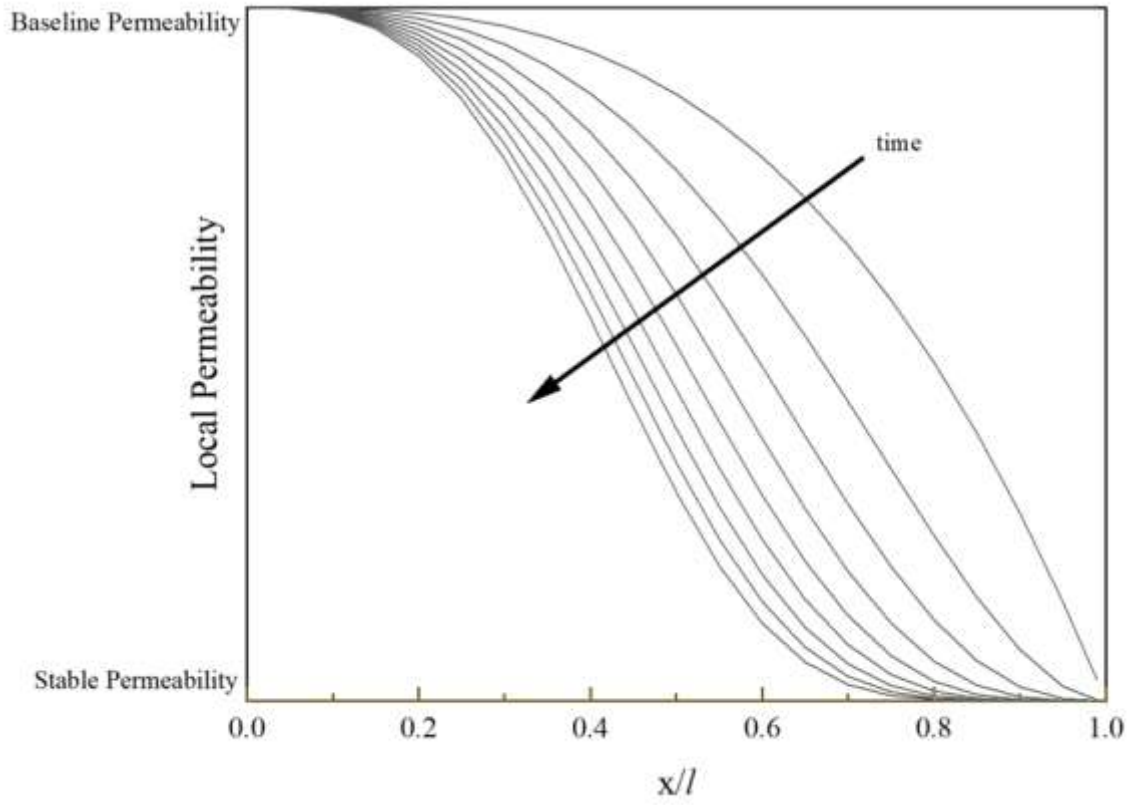

Figure 6.3. Local permeability vs. a particular point, *x*, in the membrane skin over time. As time goes on, the local permeability curve in the membrane begins to stabilize, with the curve changing less and less per unit time. This curve assumes the concentration in the upstream is high enough to essentially maintain constant local permeability.

a)

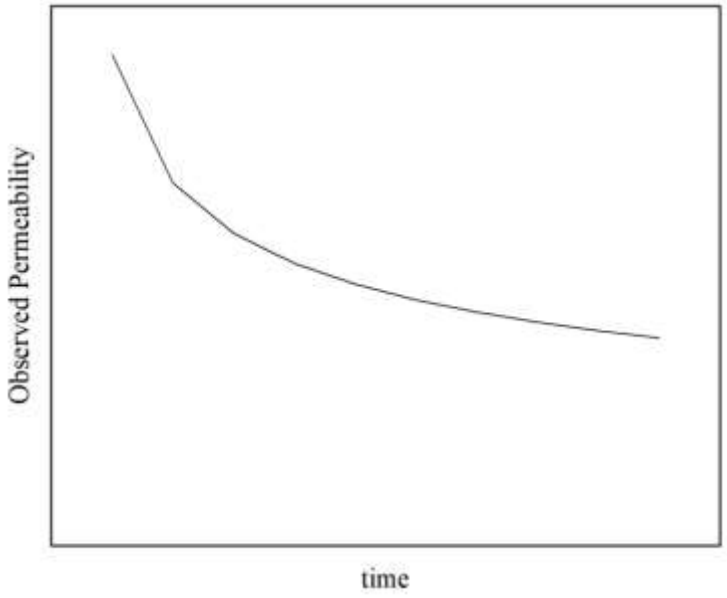

b)

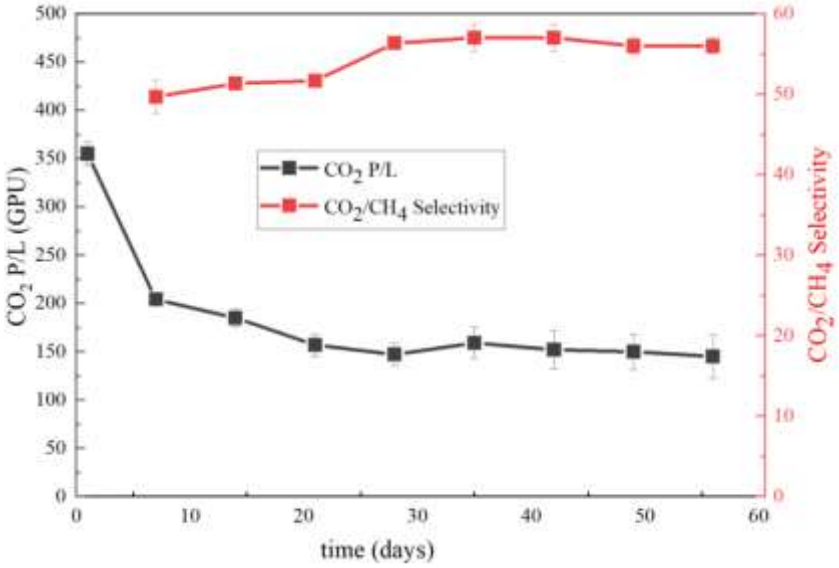

Figure 6.4. a) Integration of Figure 6.3 leads to self-retarding physical aging. b) Similar behavior is observed during actual measurements. A long-term constant-pressure permeation test performed using a 50:50 CO_2/CH_4 mixture with a 300 psia upstream at 35 °C showed self-retarding aging behavior, seemingly approaching a steady-state permeance around day 30.

If correct, this insight can also be used to shed light on C_3H_6 regeneration. It is currently hypothesized that C_3H_6, (and C_3H_8), regeneration is able to slightly reopen *slit bypass pores* that have partially closed during physical aging. Additionally, in all regeneration attempts, the permeance was never completely restored, with a significant percentage still lost due to aging. Relating this observation with the Lennard-Jones potential discussion in Section 4.4.2, it may be that the lost permeance is due to *slit bypass pores* that have aged significantly, putting them low in the potential energy well and thus making them more stable. As mentioned above, it is also hypothesized that there is a gradient of aging occurring in the CMS due to the concentration gradient. What these statements would suggest is that the effectiveness of C_3H_6 regeneration is related to the specific aging gradient in the selective skin, and thus if two sets of CMS membranes were aged differently but showed roughly similar permeance in that aged state, it is possible that after regeneration, they would have significantly different permeances.

This hypothesis can be tested if one set of CMS membrane modules is aged moderately on both sides of the membrane, while another set of CMS membrane modules is aged harshly only on one side of the membrane, thus producing two different aging gradients. As the observed permeability, or permeance, is the area under the local permeability curve normalized by the skin thickness, it is possible for these two sets of modules to have the same observed permeability, but very different local permeability curves within the skin. The current hypothesis would predict different amounts of regeneration occurring, with the modules aged on both sides of the membrane predicted to see a much more pronounced regeneration effect.

6.3.2 Future Work for Dual-mode Transport in Carbon Molecular Sieve Membranes

As mentioned in Chapter 5, it is believed that F increases with increasing partial pressure to counteract the decrease from the term $1/(1 + \sum b_i f_i)$. The dependence of F with partial pressure requires further work. Determining this dependence will ideally allow for accurate prediction of mixed gas permeabilities for a multitude of different feed conditions.

Additionally, an important aspect of this dual-mode work is the possibility of new CMS tuning techniques. Theoretically, by controlling the ratio of the two modes, a single CMS membrane type can be altered for a specific separation. It is currently hypothesized that lengthening the duration of the temperature soak during CMS formation will minimize the continuous mode by allowing more strands to be accommodated into ultramicroporous plates. This, in turn, should have an effect both on the observed sorption isotherm as well as pressure-dependence during permeation. If correct, this would shed important light on the presence of dual-mode transport in CMS membranes.

6.3.3 Combining Dual-mode transport and Physical Aging in Carbon Molecular Sieve Membranes

For a self-consistent understanding of CMS membranes, both ideas, (the proposed model for physical aging and dual-mode transport), must fit together cohesively. This cannot be done without further work. However, several hypotheses are presented here that can attempt to guide future paths.

The continuous phase in CMS is believed to consist of randomly oriented strands not incorporated to existing plates. This was hypothesized to be due to kinetic limitations,

(or limited strand mobility). This limited mobility occurs at very high temperatures, (>500 °C), implying that the strands have even more limited mobility at room temperature, or the testing temperature of 35 °C. This suggests that the continuous mode is more or less constant once it has cooled after pyrolysis and should not change drastically during aging.

As mentioned previously, several dual-mode transport models exist capable of describing trends observed in membranes. Paul & Koros proposed the first instance of such a model, followed by several additions by Barrer, Sada, and others[6, 7, 8, 9, 10, 11]. One of the important contributions of later theories, first published by Barrer, is the proposal of intra- and inter-mode jumps [11]. As local equilibrium of sorbates must be maintained, penetrants must be continuously exchanged between the two modes. This model can be simplified to a form resembling the form used in Chapter 5, specifically Equation 5.3.

What this implies then is that D_C and D_L are made up of terms representing interchange between the two modes. So the continuous mode may remain unchanged, but diffusion in and out of the continuous mode is predicted to change with aging due to the proposed tightening of ultramicropores in the Langmuir mode. Evidence demonstrating this hypothesis incorrect might imply such things as greater mobility of strands in the continuous mode or that inter-mode jumps are much less frequent than intra-phase jumps in the continuous mode, making D_{LC} and D_{CL} less impactful.

Regardless, determining how the continuous mode relates to changes during physical aging will only strengthen the understanding of transport through the complex CMS structure.

6.4 References

1. Jones CW, Koros WJ. Carbon molecular sieve gas separation membranes-II. Regeneration following organic exposure. *Carbon* 1994, **32**(8)**:** 1427-1432.

2. Xu L, Rungta M, Hessler J, Qiu W, Brayden M, Martinez M, *et al.* Physical aging in carbon molecular sieve membranes. *Carbon* 2014, **80:** 155-166.

3. Fu S, Sanders ES, Kulkarni SS, Koros WJ. Carbon molecular sieve membrane structure–property relationships for four novel 6FDA based polyimide precursors. *Journal of Membrane Science* 2015, **487:** 60-73.

4. Petropoulos J. Quantitative analysis of gaseous diffusion in glassy polymers. *Journal of Polymer Science Part A-2: Polymer Physics* 1970, **8**(10)**:** 1797-1801.

5. Crank J. *The mathematics of diffusion*. Oxford university press, 1979.

6. Paul DR, Koros WJ. Effect of partially immobilizing sorption on permeability and the diffusion time lag. *Journal of Polymer Science: Polymer Physics Edition* 1976, **14**(4)**:** 675-685.

7. Koros WJ, Chern RT, Stannett V, Hopfenberg HB. A model for permeation of mixed gases and vapors in glassy polymers. *Journal of Polymer Science: Polymer Physics Edition* 1981, **19**(10)**:** 1513-1530.

8. Sada E, Kumazawa H, Yakushiji H, Bamba Y, Sakata K, Wang ST. Sorption and diffusion of gases in glassy polymers. *Industrial & Engineering Chemistry Research* 1987, **26**(3)**:** 433-438.

9. Sada E, Kumazawa H, Xu P, Nishigaki M. Mechanism of gas permeation through glassy polymer films. *Journal of Membrane Science* 1988, **37**(2)**:** 165-179.

10. Fredrickson GH, Helfand E. Dual-mode transport of penetrants in glassy polymers. *Macromolecules* 1985, **18**(11)**:** 2201-2207.

11. Barrer RM. Diffusivities in glassy polymers for the dual mode sorption model. *Journal of Membrane Science* 1984, **18:** 25-35.

APPENDIX A

BRIEF INVESTIGATION INTO REMOVAL OF ISO-PENTANE

As mentioned in Section 4.2.2, n-pentane was found to be very difficult to remove from CMS hollow fibers. After exposure and subsequent regeneration, the membrane had lost 30% of its CO_2 permeance and the CO_2/CH_4 selectivity had increased 29%. Removal of n-hexane was significantly more effective, as the membrane before and after exposure to n-hexane was essentially the same. This suggested that there was still pentane sorbed in the CMS membrane.

Pentane, in addition to CMS, has also been shown to be very difficult to remove from fullerene. Work by Pekker et al. suggests the formation of a clathrate between n-pentane and a fullerene crystal, highlighted in Figure A.1 [1]. This is not to say that the structure of CMS resembles the extremely ordered structure of crystalized fullerene; however, the formation of a fullerene – n-pentane clathrate does rely on the existence of ~10 angstrom pores, which has shown to be present in 6F-derived CMS membranes [Koros Adams 2019]. The work presented by Pekker et al. also mentions that the clathrate does not form when i-pentane is used instead of n-pentane, suggesting that i-pentane might be able to be removed from CMS membranes. This hypothesis was tested using the same experimental procedure outlined in Section 4.2.2 for n-pentane exposure and accompanying C_3H_6 regeneration.

Interestingly, Figure A.2 demonstrates significant ease of removal of i-pentane with only a 12% drop in CO_2 permeance and about a 1% increase in CO_2/CH_4 selectivity. This is much better than the n-pentane case, which showed a 30% drop in CO_2 permeance

and a 29% increase in CO_2 selectivity. These data are insightful in suggesting some interesting interaction between n-pentane and 6F-derived CMS membranes, however more work is required to determine the legitimacy and the intricacies of this relationship.

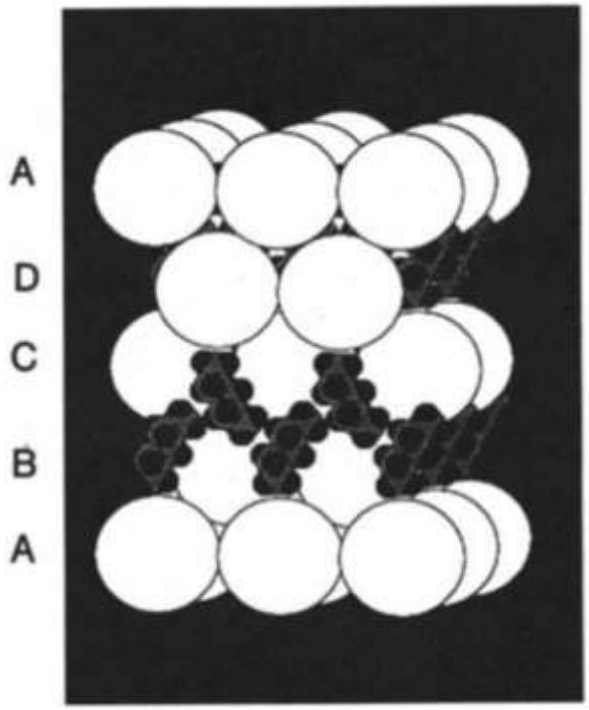

Figure A.1. Packing of n-pentane molecules in orthorhombic unit cell of fullerene[1].

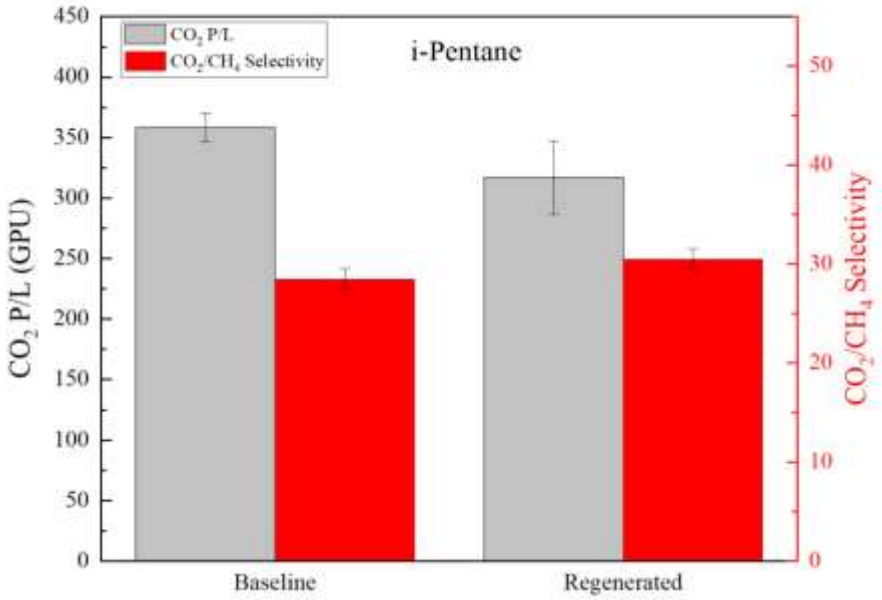

Figure A.2. CO_2 permeance and CO_2/CH_4 selectivity for baseline and regenerated 6F-derived 550 °C UHP Ar CMS hollow fiber membranes. C_3H_6 regeneration performed for 72 hours after exposure i-pentane for 24 hours. All permeation tests performed at 35 °C using an upstream pressure of 100 psia 50:50 CO_2/CH_4 and downstream pressure of 0 psia.

References

1. Pekker S, Faigel G, Fodor-Csorba K, Granasy L, Jakab E, Tegze M. Structure and stability of crystalline C60· n-pentane clathrate. *Solid state communications* 1992, **83**(6)**:** 423-426.

APPENDIX B

AUXILIARY CHARACTERIZATION TECHNIQUES

This appendix shows results from several characterization techniques performed on fresh and aged CMS samples. The operating conditions of the following characterization techniques are described in Section 3.4.4. As shown in the figures below, minimal to no change was observed in the sample after the 1-week vacuum exposure. This suggests that the changes to the CMS structure are very subtle. Additionally, it reiterates that traditional characterization techniques useful for more organized rigid sieves, like MOFs and zeolites, are not as useful for the highly amorphous CMS membrane. Trends from transport are, at least at this point, the most powerful tool available to gaining insight into the CMS structure.

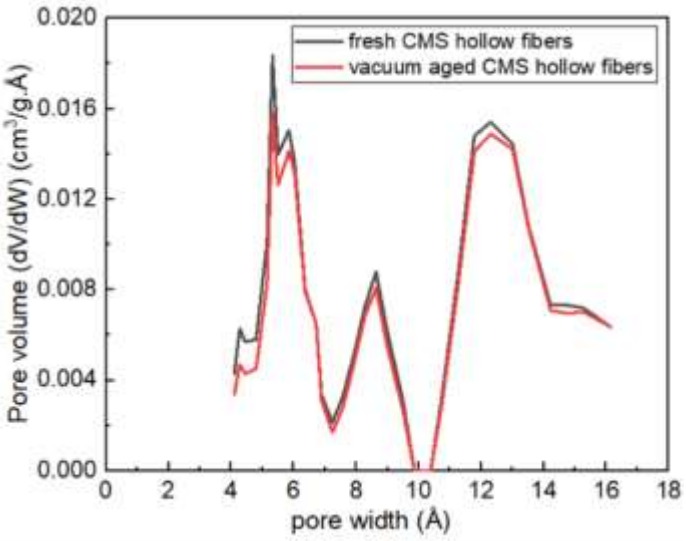

Figure B.1. CO_2 physisorption results at 0 °C on fresh and aged hollow fiber CMS samples. The sample was aged for 1 week under vacuum.

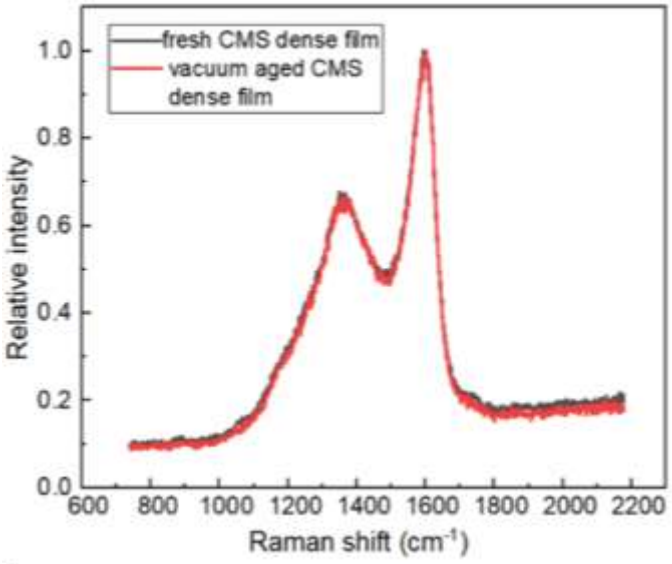

Figure B.2. Raman spectroscopy results on fresh and aged dense film CMS membranes. The dense film sample was aged for 1 week under vacuum.

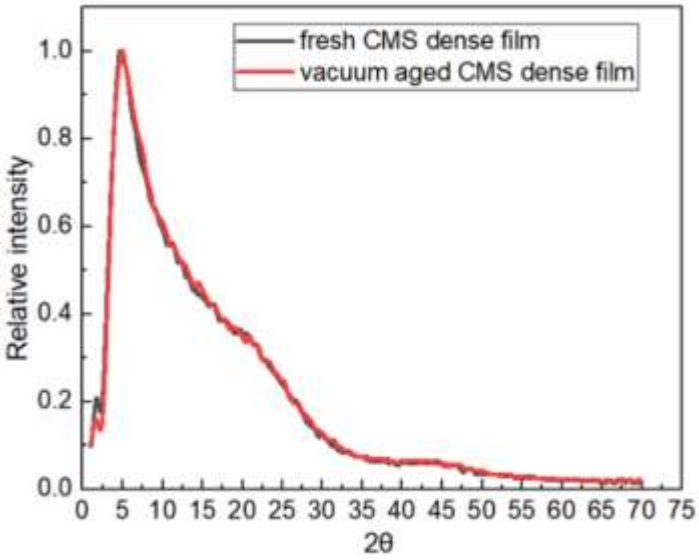

Figure B.3. X-ray diffraction results on fresh and aged dense film CMS membranes. The dense film sample was aged for 1 week under vacuum.

APPENDIX C

DUAL-MODE FITTING CONSTANTS FOR 6F-DERIVED 550 °C UHP AR CMS MEMBRANES

Table C.1. Dual-mode fitting constants for several constituents on 6F-derived 550 °C UHP Ar CMS membranes.

Penetrant	Temperature (°C)	Membrane Form	$k_{C,i}$ $\frac{cm^3(STP)}{cm^3\ cmHg}$	$C'_{L,i}$ $\frac{cm^3(STP)}{cm^3}$	b_i $cmHg^{-1}$	K_i -
CO_2	35	Hollow Fiber	0.041 ± 0.002	103.5 ± 4.3	0.013 ± 0.003	32.2 ± 6.4
	25	Hollow Fiber	0.041	115.4	0.014	40.9
CH_4	35	Hollow Fiber	0.049 ± 0.002	61.3 ± 1.7	0.007 ± 0.002	8.3 ± 2.0
C_3H_6	35	Hollow Fiber	0.046 ± 0.003	83.0 ± 2.0	0.330 ± 0.044	599 ± 23
	25	Dense Film	0.042	85.1	0.612	1243
n-C_5H_{12}	25	Hollow Fiber	0.019	53.9	3.84	11100
n-C_6H_{14}	25	Hollow Fiber	0.196	57.7	10.2	3012

APPENDIX D

SCANNING ELECTRON MICROGRAPHS OF 6F PRECURSORS AND 6F-DERIVED CMS HOLLOW FIBER MEMBRANES

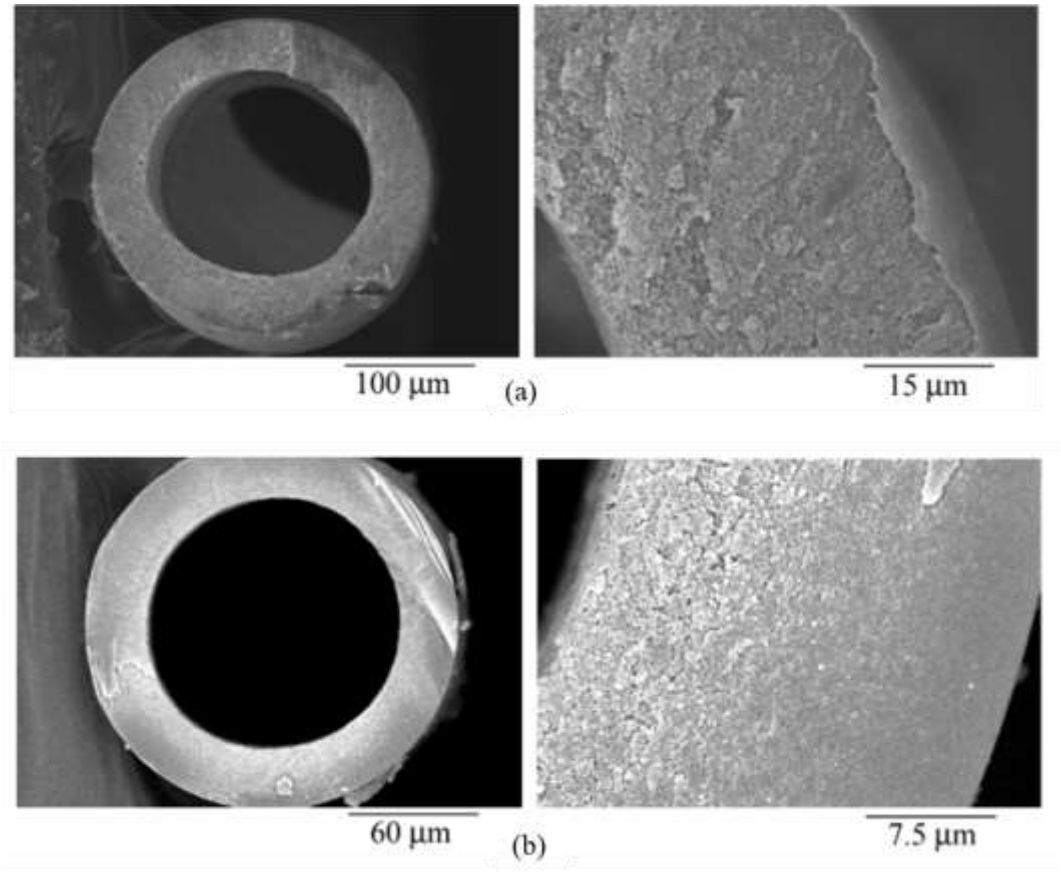

Figure D.1. Scanning electron micrographs of (a) 6F polymer precursors and (b) 6F-derived CMS hollow fiber membranes[1].

References

1. Vu DQ. Formation and characterization of asymmetric carbon molecular sieve and mixed-matrix membranes for natural gas purification. 2003.